Astrocytes mediate neurovascular signaling to capillary pericytes but not to arterioles

Anusha Mishra[1], James P. Reynolds[2], Yang Chen[1], Alexander V. Gourine[1],

Dmitri A. Rusakov[2] and David Attwell[1]

[1]Department of Neuroscience, Physiology & Pharmacology and [2]Institute of Neurology

University College London

London, UK

Correspondence to DA, d.attwell@ucl.ac.uk

Abstract

Active neurons increase their energy supply by dilating nearby arterioles and capillaries. This neurovascular coupling underlies BOLD functional imaging signals, but its mechanism is controversial. Canonically, neurons release glutamate to activate metabotropic glutamate receptors (mGluR5) on astrocytes, evoking Ca^{2+} release from internal stores, activating phospholipase A_2 and generating vasodilatory arachidonic acid derivatives. However, adult astrocytes lack mGluR5, and knock-out of the IP_3 receptors that release Ca^{2+} from stores does not affect neurovascular coupling. We now show that buffering astrocyte Ca^{2+} inhibits neuronally-evoked capillary dilation, that astrocyte $[Ca^{2+}]_i$ is raised not by release from stores but by entry through ATP-gated channels, and that Ca^{2+} generates arachidonic acid via phospholipase D2 and diacylglycerol kinase rather than phospholipase A_2. In contrast, dilation of arterioles depends on NMDA receptor activation and Ca^{2+}-dependent NO generation by interneurons. These results reveal that different signalling cascades regulate cerebral blood flow at the capillary and arteriole levels.

Introduction

Functional hyperemia is the phenomenon by which active brain regions induce a local increase in blood flow to match their energy demands, via a process termed neurovascular coupling. Traditionally, regulation of cerebral blood flow was thought to occur at the level of arterioles[1-3], however, capillaries in the brain are also wrapped by contractile cells called pericytes[4], which can respond to neuronal activity and control blood flow at a more local level than arterioles[5,6]. Although neurovascular coupling is the basis of blood oxygen level dependent (BOLD) functional magnetic resonance imaging (fMRI), an increasingly routine method used to measure brain activity in the clinic and in cognitive studies, our understanding of the underlying signalling mechanisms is still incomplete.

Neurovascular coupling can partly occur as a result of direct signalling from neurons to the vasculature[7]. However, over the last decade, a role for astrocytes, which have endfoot processes near blood vessels, has also been demonstrated, whereby neurons signal to astrocytes, which in turn release vasoactive substances onto vessels[8]. Initial data suggesting astrocyte-mediated neurovascular signalling came from experiments in which stimulating neurons led to a rise in astrocyte $[Ca^{2+}]_i$ as well as arteriole dilation[1]. It was further shown that raising astrocyte $[Ca^{2+}]_i$ evoked vascular dilations and constrictions[2,3,9], which were produced by metabolites of arachidonic acid (AA) generated by phospholipase A_2 (PLA_2). Dilation occurred via the formation of prostaglandin E_2 (PGE_2) and epoxyeicosatrienoic acids (EETs), while production of 20-hydroxyeicosatetraenoic acid (20-HETE) resulted in constriction (see ref. 8 for review).

Although these findings were obtained in several laboratories, controversies still abound. Astrocyte Ca^{2+} signals may be too small or slow[10], or too infrequent[11], to have a causative role in neurovascular coupling. However, these conclusions were based on measuring Ca^{2+} signals within astrocyte cell bodies, rather than in the fine processes[12] of astrocytes near synapses which are presumably the first responders to neuronal activity. Indeed, recent *in vivo* studies have reported rapid, physiological stimulation-evoked $[Ca^{2+}]_i$

rises in astrocyte somata and endfeet in the somatosensory cortex[13], and in the processes but not the somata of olfactory bulb astrocytes[14].

A second controversy concerns how elevations of astrocyte Ca^{2+} concentration are generated. While these were originally thought to reflect activation of mGluR5 and downstream IP_3-dependent release of Ca^{2+} from internal stores[1-3], recent studies show that mGluR5 expression is downregulated in astrocytes from adult animals[15]. Furthermore, animals lacking IP_3R_2, the primary IP_3 receptor in astrocytes, display unaltered neurovascular coupling[16]. Nevertheless, there are other mechanisms which could raise astrocyte $[Ca^{2+}]_i$, including Ca^{2+} permeable AMPA receptors[17], NMDA receptors[18], ATP receptors[19] and TRPA1 channels[20], and thus mediate astrocyte to vessel signalling.

Finally, it is unclear whether neurovascular coupling at the capillary level is mediated by the same pathways as that at the arteriole level. Although dilation of capillaries and arterioles both rely on relaxation of actomyosin, in pericytes and in arteriolar smooth muscle respectively, it seems plausible that local (capillary) and spatially broader (arteriolar) control of blood flow might be driven by different signalling pathways.

Here, we investigated the role of astrocytes in mediating neurovascular coupling in the cerebral cortex, in brain slices and *in vivo*. We provide the first direct demonstration that a rise in astrocyte $[Ca^{2+}]_i$ is necessary for neuronally-evoked capillary dilation to occur. We show that the source of Ca^{2+} involved in this process and its molecular effects are radically different from what was previously believed. We also show that arteriole dilation is not mediated by astrocyte Ca^{2+} signalling, but instead depends on NMDA receptor-mediated nitric oxide release (Supp. Fig. 1).

Results

Neuronal activity evokes capillary dilation

We assessed whether cerebral cortical capillaries can respond to electrically stimulated synaptic activity in cortical slices from P21 (adolescent) rats. Stimulation-evoked fibre volley and field excitatory post-synaptic currents (fEPSCs) were recorded in all

experiments to confirm activation of the neuropil near the capillary being studied (Supp. Fig. 2). Vascular responses are known to be modulated by the oxygen (O_2) concentration in the tissue: physiological [O_2] produced by bubbling the superfusate with 20% O_2 results in larger dilations[6,9,21]. Therefore, all experiments reported here were conducted using 20% O_2. Furthermore, since vessels in brain slices do not have resting tone due to a lack of noradrenergic signalling from the locus coeruleus, and a lack of perfusion pressure and blood flow, a vasoconstricting agent is required to provide the resting tone upon which neuronally-evoked dilations normally occur[22]. Here, we bath-applied the thromboxane A_2 analogue U46619 (200 nM) for at least 5 minutes to pre-constrict cortical vessels prior to neuronal stimulation. Capillaries were identified as vessels <10 µm wide that lack a continuous layer of smooth muscle[22] (Supp. Fig. 2). U46619 constricted capillaries by 18.7±0.7% (n=213 separate capillary regions (presumed locations of pericytes) in 112 vessels from 70 animals: Fig. 1a-b; Supp. Fig. 3) within minutes, without affecting electrically-evoked synaptic activity (Supp. Fig. 2c-d), and this constriction was maintained for at least 30 min (Supp. Fig. 3a). Electrically-stimulated neuronal activity then dilated the capillaries by 14.5±0.5% (Fig. 1a, b).

We first confirmed that stimulation-evoked capillary dilation resulted from neuronal activity and not direct stimulation of the vasculature. In the presence of tetrodotoxin (TTX, 500 nM), stimulation-evoked neuronal activity (the fibre volley and fEPSCs) was completely abolished (Supp. Fig. 2c) and capillary responses were also absent (0.2±1.6% dilation, n=11; Fig. 1c, f) unlike for interleaved controls (14.0±1.6% dilation, n=7, significantly different, p=0.00008; Fig. 1f). Blocking ionotropic glutamate receptors showed that post-synaptic activity was necessary for neurovascular signalling to capillaries. The AMPA/KA receptor blocker NBQX (10 µM) inhibited stimulation-evoked fEPSCs (Supp. Fig. 2c, d) and reduced capillary dilation by 82.2% (p=0.002; Fig. 1d, g). In contrast, the NMDA receptor blocker D-AP5 (25 µM) had no effect on stimulation-evoked capillary dilation (p=0.6; Fig. 1e, h). Thus, stimulation-evoked capillary dilation reflects action potential driven glutamatergic synaptic activity but does not depend on Ca^{2+} entry into neurons via NMDA receptors.

Capillary dilation is mediated by Ca^{2+}-dependent astrocyte signalling

We next investigated whether astrocyte Ca^{2+} signalling mediates neuron-to-capillary signalling. To address this, astrocytes near the vessel of interest were whole-cell patch-clamped and dialyzed with either a control internal solution containing 1 mM EGTA (ethylene glycol-bis(2-aminoethylether)-N,N,N',N'-tetraacetic acid) or one containing 30 mM of the faster Ca^{2+} chelator BAPTA (1,2-bis(2-aminophenoxy)ethane-N,N,N′,N′-tetraacetic acid). Spread of the pipette solution between astrocytes via gap junctions was visualized using the dye Alexa Fluor 488 (40 μM). After 10-15 minutes of dialysis, the astrocyte network, including endfeet along the vessel of interest, was filled with Alexa Fluor 488 (Fig. 2a). Stimulating neuronal activity when astrocytes were dialyzed with the control (EGTA) internal solution evoked robust capillary dilations (16.2±1.7%, n=12; Fig. 2b, c). However, when astrocytes were dialyzed with BAPTA to buffer rises in $[Ca^{2+}]_i$, stimulation-evoked dilation was reduced by 64% to 5.9±2.0% (n=17, p=0.0007; Fig. 2b, c). The free $[Ca^{2+}]_i$ in both the EGTA and BAPTA internal solutions was set to ~24 nM, so the effects observed are not attributable to differences in baseline free $[Ca^{2+}]_i$, implying that a transient rise in astrocyte $[Ca^{2+}]_i$ in response to neuronal stimulation is, at least in part, necessary for neurovascular signalling to capillaries.

In some experiments, we imaged vessels as the internal solution spread from the patch-clamped astrocyte into the endfoot processes, to observe whether buffering astrocyte Ca^{2+} rises had any effect on baseline capillary diameter. There was no significant change in the baseline diameter of the vessels when using either the control internal solution (2.0±1.8% constriction in 4 capillaries, not significantly different from zero, p=0.3) or the BAPTA internal (5.4±3.2% dilation in 8 capillaries; not significantly different from zero, p=0.1; diameter change in BAPTA was not significantly different from that in EGTA, p=0.2).

$P2X_1$ receptors raise astrocyte $[Ca^{2+}]_i$

Many mechanisms leading to a $[Ca^{2+}]_i$ rise in astrocytes have been suggested. Group I metabotropic glutamate receptors (mGluR1/5)[23] and the ATP receptor $P2Y_1$[24] are both G-protein coupled receptors (GPCRs) associated with $G_{\alpha q}$ signalling that induces Ca^{2+} release

from internal stores by generating IP_3. In particular, mGluR1/5 receptors have long been thought to be the primary cause of astrocyte $[Ca^{2+}]_i$ rises[23]. Recently, group II mGluRs were also shown to raise $[Ca^{2+}]_i$ within astrocytes via an as yet undefined mechanism[25]. Furthermore, the Ca^{2+}-permeable heteromeric ATP receptor $P2X_{1/5}$[19] and transient receptor potential A1 (TRPA1) channels[20] are also possible routes for Ca^{2+} influx into astrocytes. We tested the role of each of these receptors in mediating capillary-level neurovascular coupling. Stimulation-evoked capillary dilation was not reduced after bath application of a non-specific blocker of both group I and II mGluRs, (S)-MCPG (1 mM, p=0.1; Fig. 2d, i), the P2Y1 receptor blocker MRS2179 (25 μM, p=0.8; Fig. 2e, j) or the TRPA1 blocker A967079 (10 μM, p=0.3; Fig. 2f, k). However, the $P2X_1$ blockers NF449 (100 nM, Supp. Table 1) and NF023 (5 μM) reduced the stimulation-evoked capillary dilation by 58% (p=0.0007; Fig. 2g, l) and 94% (p=0.001; Supp. Fig. 4d), respectively. Similar results were obtained using shorter stimulation durations than the 1 min used above (NF449 reduced dilation by 94% (p=0.005) and 60% (p=0.01) for 200 ms and 5 s stimulation, respectively; Supp. Fig. 4a-c), and in P45 mice (66% reduction with NF449, p=0.00008 using 5 s stimulation; Supp. Fig. 4e). If $P2X_1$ receptors raise astrocyte $[Ca^{2+}]_i$ to evoke the dilation, then we should also be able to evoke dilation simply by activating this receptor. Indeed, a 5 s puff application of α,β-methylene ATP (100 μM, see Methods), an agonist for $P2X_1$[26], onto the neuropil induced a 10.7±2.3% dilation of cortical capillaries, whereas application of vehicle did not (0.4±1.3% constriction, significantly different, p=0.0007; Fig. 2h, m). These data suggest that capillary level neurovascular coupling occurs largely through a $P2X_1$ receptor-dependent pathway in astrocytes.

To study stimulation-evoked changes in $[Ca^{2+}]_i$ within astrocyte endfeet, we whole-cell clamped astrocytes to selectively fill them with the membrane-impermeant Ca^{2+} indicator dye Fluo4 (50 μM), and a reference dye (Alexa Fluor 594, 40 μM) to allow ratiometric imaging (as *R=(Fluo4 intensity)/(Alexa Fluor 594 intensity)*). We observed spontaneous local Ca^{2+} transients in astrocyte cell bodies and processes, as previously reported[27-29]. Stimulating neuronal activity evoked an increase in $[Ca^{2+}]_i$ in astrocytes (ΔR/R=41.4±11.7% in endfeet,

n=9, p=0.003 compared to zero; ΔR/R=58.4±20.2% in processes, n=23, p=0.006; ΔR/R=60.2±24.3% in somata, n=13, p=0.02; Fig. 3a-c). The amplitude of this signal was reduced by 81% and 85% in endfeet and processes, respectively, by the $P2X_1$ receptor blocker NF449 (ΔR/R=7.9±3.1% in endfeet, n=6, p=0.02 compared to control data; ΔR/R=8.5±3.4% in processes, n=14, p=0.02; Fig. 3b, c). NF449 did not significantly block the calcium rise in somata (Fig. 3c). These data are consistent with $P2X_1$ receptor-mediated signalling within astrocytes mediating the capillary dilations seen in Figs. 1 and 2. In contrast, the mGluR blocker (S)-MCPG (1 mM) did not alter the $[Ca^{2+}]_i$ changes in the endfoot, process or somata (Fig. 3c).

Arachidonic acid metabolites mediating capillary dilation

Astrocyte-mediated neurovascular coupling is thought to occur via the synthesis of AA by Ca^{2+}-activated phospholipase A_2 followed by metabolism into vasoactive substances[8] such as prostaglandins (by the activity of cyclooxygenase (COX)) or EETs (by the activity of epoxygenases). We tested the contribution of these enzymes using specific inhibitors. The COX1 inhibitor SC-560 (1 μM) reduced the stimulation-evoked capillary dilation by 64% (p=0.0002; Fig. 4a, d), but the COX2 inhibitor NS-398 (10 μM; Fig. 4b, e) and the epoxygenase inhibitor PPOH (25 μM; Fig. 4c, f) had no effect on the dilation. COX1 generates several prostaglandin derivatives, including the vasodilators PGE_2 and PGI_2. Blocking the EP_4 receptor for PGE_2 with L-161,982 (1 μM) reduced the stimulation-evoked dilation by 72% (p=0.004; Fig. 4g, j). In contrast, blocking the IP receptor for PGI_2 with CAY10441 (1 μM) did not affect the dilation (Fig. 4h, k). Nitric oxide (NO) has also been shown to contribute to arteriolar vasodilation in the cortex[30,31], however, when the NO synthase inhibitor L-N^G-nitroarginine (L-NNA; 100 μM) was applied, stimulation-evoked capillary dilation was not reduced (Fig. 4i, l), implying that NO does not contribute to capillary dilation in the cortex. Thus, PGE_2 generated by COX1 and acting on EP_4 receptors is the primary vasoactive signal mediating capillary dilation.

We used immunohistochemistry to investigate the cellular location of the enzymes metabolising AA. We found COX1 labelling in processes along arterioles and capillaries that

co-labelled for aquaporin 4 (AQP_4), a protein expressed highly in astrocyte endfeet (Supp. Fig. 5a). In contrast, COX2 did not colocalize with the astrocyte structural protein glial fibrillary acidic protein (GFAP), but was expressed diffusely in the neuropil with higher expression in neuronal somata (Supp. Fig. 5b). Antibodies against the CYP2C11 isoform of epoxygenase, reported to be the predominant epoxygenase in the rodent brains[32], labelled AQP_4-expressing endfeet along larger vessels, but not along capillaries (Suppl. Fig. 5c). Furthermore, antibodies against PGE_2 synthase (PGES) also labelled GFAP-expressing astrocyte cell bodies, processes and endfeet (Supp. Fig. 5d). These findings are consistent with the functional data in Fig. 4 suggesting that PGE_2 is the main vasoactive metabolite of AA that signals to capillaries, and is synthesized within astrocytes.

PLD2, not PLA_2, initiates neurovascular coupling at the capillary level

The Ca^{2+}-dependent enzyme PLA_2 is thought to synthesize the AA which is converted into PGE_2[2,8,33]. We found that PLA_2 immunolabelling colocalized with GFAP positive astrocyte endfeet along capillaries (Supp. Fig. 6), suggesting a possible role for this enzyme. Surprisingly, however, stimulation-evoked capillary dilation was unchanged when PLA_2 was blocked with its inhibitor MAFP (10 μM, Fig. 5a, d). Thus, despite being in the correct cellular compartment, PLA_2 is not the primary enzyme involved in the AA synthesis required for signalling to capillaries. We therefore sought other possible AA sources.

The enzymes phospholipase C (PLC) and PLD can produce AA via a multi-step process. PLC breaks down PIP_2 (phosphatidylinositol 4,5-bisphosphate) to DAG (diacylglycerol) and IP_3, while PLD acts on membrane phospholipids to synthesize phosphatidic acid, which is then converted to DAG by phosphatidate phosphatase. DAG produced by PLC or PLD in this way can be further metabolized by DAG lipase (DAGL) to produce AA. A specific blocker of PLC, U73122 (10 μM), did not reduce stimulation-evoked capillary dilation (Fig. 5b, e). In contrast, a PLD specific blocker FIPI (1 μM) reduced dilation by 64% ($p=0.0005$; Fig. 5c, f), suggesting that PLD plays a major role in synthesising AA. Two isoforms of PLD are expressed in mammals, PLD1 and PLD2, both of which are regulated[34,35] by Ca^{2+}. A specific inhibitor of PLD1, VU0155069 (500 nM), had no effect on

stimulation-evoked dilation (Fig. 5g, j), however, a blocker of PLD2, CAY10594 (1 μM) completely abolished the capillary dilation (p=0.0002; Fig. 5h, k), suggesting that AA synthesis is PLD2 dependent. If so, then the downstream enzyme DAGL, which is required for AA production from DAG, should also be involved. Indeed, the DAGL inhibitor RHC80267 (50 μM) also blocked the stimulation-evoked capillary dilation (reduced by 81%, p=0.0004; Fig. 5i, l), suggesting the PLD2-DAGL pathway as the mechanism for AA synthesis.

We considered whether PLD2 might, instead of being in the pathway for AA synthesis, be activated downstream of the PGE_2 receptor EP_4 in pericytes to cause the capillary dilation. However, there was no difference between PGE_2-induced dilation of cortical capillaries in the absence (8.1±1.7%) and presence (8.5±2.1%) of the PLD blocker FIPI (Supp. Fig. 7), supporting our conclusion that the PLD2-DAGL pathway is upstream of AA synthesis.

Consistent with these results, immunolabelling for PLD1 showed that it is expressed diffusely in the neuropil and strongly in endothelial cells lining arterioles (Supp. Fig. 8a), but it was not in astrocyte endfeet, pericytes or capillary endothelial cells (Supp. Fig. 8a, b). In contrast, PLD2 immunolabelling occurred in GFAP-positive astrocyte endfeet on capillaries (Supp. Fig. 8c) and cell bodies (Supp. Fig. 8d), but not in pericytes or endothelial cells, consistent with a role in astrocyte-mediated neurovascular signalling to capillary pericytes.

Arteriole dilation is mediated by a different signalling pathway

To compare the data above on capillary dilation with the dilation of arterioles evoked by neuronal activity, we carried out similar experiments imaging arterioles. U46619 preconstricted arterioles by 11.8±0.8% (n=36 arterioles from 26 animals, Supp. Fig. 9). The neuronal stimulation-evoked dilation of arterioles (7.0±0.7%, n=36, mean of all control data in Fig. 6) was smaller than that evoked in capillaries (12.1±1.9%, Supp. Fig. 4b, both with 5 s stimulation). Remarkably, in contrast to the capillary dilation, the arteriole dilation was unaffected by dialysing the astrocyte network with BAPTA (Fig. 6a, b) or by blocking $P2X_1$ receptors, PLD2 or PLA_2 (Fig. 6c-e, h-i), indicating that a completely different signalling pathway, independent of astrocyte $[Ca^{2+}]_i$ changes, mediates arteriole dilation. However,

again unlike the capillary dilation (Figs. 1h, 4l), arteriole dilation was strongly inhibited by blocking NMDA receptors (p=0.008, Fig 6 f, j) or NO synthase ($p=10^{-6}$, Fig. 6g, k).

Neurovascular signalling *in vivo*

To determine whether the ATP-dependent astrocyte signalling mechanism also mediates neurovascular coupling at the capillary level *in vivo*, we used 2-photon excitation fluorescence microscopy to image cortical capillaries and arterioles *in vivo* in anesthetised rats, with intravascular FITC-dextran to visualise the blood vessels (Fig. 7a-b, see Methods). We evoked neuronal activity in the somatosensory cortex by electrically stimulating the forepaw. The diameter of all imaged capillaries was 6.7±0.2 μm (n=102) and of arterioles was 13.4±0.5 μm (n=77). Forepaw stimulation evoked a dilation in 22% of capillaries and 24% of arterioles (Fig. 7c-e). In those vessels, capillary dilation averaged 29.3±5.8% and arteriole dilation averaged 10.9±2.2% (Fig. 7f).

Local infusion of the $P2X_1$ blocker NF449 (5 μM) into the cortical region did not significantly affect the percentage of capillaries dilating (reduced to 13%, p=0.3, Fig. 7e). However, the capillary dilations that did occur were reduced by 68% in size to 9.5±1.8% (p=0.006, Fig. 7d, f). In contrast, NF449 did not significantly alter either the percentage of dilating arterioles (18%, p=0.6) or the magnitude of the arteriole dilations (9.7±1.7%, p=0.7; Fig. 7c, e-f), just as in slices (Fig. 6h).

Discussion

Neurovascular coupling plays a crucial role in controlling cerebral blood flow, both physiologically and in disease. Capillary dilation generates a large portion of the blood flow increase evoked by neuronal activity, and thus is expected to contribute significantly to the BOLD signal[6]. In ischemia, pericytes constrict capillaries, contributing to the lack of reperfusion of the microvasculature that occurs after a thrombus is removed from an upstream artery[6,36]. Consequently, characterising the signalling mechanisms that regulate capillary and arteriole dilation is important for understanding the blood flow response to physiological activity and to disease. In this study, we have demonstrated that neurovascular coupling at the capillary and arteriole levels differ mechanistically (Supp. Fig. 1). Neurovascular coupling at the capillary level is largely dependent on astrocyte Ca^{2+} signalling, and our data reveal a new mechanism by which astrocytes alter their $[Ca^{2+}]_i$ in response to neuronal activity: influx of Ca^{2+} via the ionotropic ATP receptor $P2X_1$. Thus astrocyte $[Ca^{2+}]_i$ can be raised without a need for mGluR5[37] and IP_3R_2 mediated signalling, which have recently been suggested to be unnecessary for neurovascular coupling in adult animals[15,16,38], and astrocyte Ca^{2+} transients observed in IP_3R_2 knockout mice[39] may partly reflect activation of $P2X_1$ receptors. Our data are consistent with work showing that overexpression of an ecto-nucleotidase (to promote rapid ATP degradation) strongly reduces BOLD fMRI signals triggered by somatosensory stimulation in rats[40]. We also show that, although signalling to capillaries is mediated by AA metabolites, the synthesis of AA depends not upon PLA_2 as generally assumed[2,8], but rather on PLD2 and DAGL activity. Furthermore, neuronal activity induced capillary dilation is unaffected by block of NO synthase (thus differing from the pericyte-mediated dilation we previously characterised in cerebellum[6], presumably because of the difference in brain region (as the cerebellum expresses more NOS) and/or because dilation was evoked by glutamate superfusion in the latter study but by endogenous glutamate release here). In contrast, neurovascular signalling to cortical arterioles is not mediated by $P2X_1$, astrocyte Ca^{2+}, PLD2 or PLA_2 but, unlike cortical capillary dilation, requires the activation of NMDA receptors and production of NO.

Our data suggest that neuronal activity results in postsynaptic neurons (Fig. 1) releasing ATP, which acts on astrocyte ATP receptors containing $P2X_1$ subunits to produce a $[Ca^{2+}]_i$ rise (Figs. 2 and 3). This activates PLD2 (Figs. 5 and Supp. Fig. 8), resulting in AA synthesis via DAGL, and downstream metabolism by COX1 into vasodilatory PGE_2, which is released onto capillary pericytes to induce dilation via the EP_4 receptor (Fig. 4, Supp. Fig. 5). $P2X_1$ receptors are expressed in cortical astrocytes along with $P2X_5$ receptors[19], which can together form heterotrimers and contribute to Ca^{2+} influx. The astrocyte Ca^{2+} influx causing capillary dilation (Figs. 2, 3, 7, Supp. Fig. 4) may be via $P2X_1$ homotrimers or $P2X_{1/5}$ heterotrimers[19], as both are blocked by NF449 and activated by α,β-methylene ATP (puffed onto the neuropil; Fig. 2h, m and Supp. Fig. 10). Although it was previously reported that ATP is released[40] from presynaptic terminals[41], we show that NBQX blocks the capillary dilation, implying that postsynaptic glutamate receptor activation is needed for ATP release, at least in the cortex. The mechanism of this ATP release has yet to be investigated.

In contrast to capillary dilation, arteriole dilation does not depend on $P2X_1$ receptors, PLA_2, PLD2 or astrocyte calcium signalling, but is dependent on NMDA receptor activation and nitric oxide synthesis (Fig. 6-7) as previously suggested[30,31]. It has been suggested that activation of NMDA receptors, by Ca^{2+}-dependent release of D-serine from astrocytes, generates NO from eNOS in endothelial cells, and thus helps to dilate penetrating arterioles[31]. Our data showing that buffering astrocyte $[Ca^{2+}]_i$ does not inhibit arteriole dilation (Fig. 6a, b) argue against a role for astrocyte Ca^{2+} in triggering arteriole dilation in our experiments, and furthermore transcriptome data suggest there are no NMDA receptors on endothelial cells[42]. We therefore assume that the NO is generated by neuronal NOS, which is Ca^{2+}-dependent and predominantly located in interneurons in the cortex[43,44].

It has previously been suggested that, in the cortex, NO release is needed to maintain neurovascular coupling but not to mediate it[45]. This is similar to the idea that, in cortex[31] and in cerebellum[6], NO serves to suppress the generation of the vasoconstrictor 20-HETE from AA while another AA derivative, PGE_2, dilates the arterioles. We have shown that blocking AA production by inhibiting PLA_2 or PLD2 has no effect on the arteriole dilation evoked by

neuronal activity (Fig. 6d, e, i), leading us to favour the idea that NO may directly mediate arteriole dilation in our preparation. However, we cannot rule out the possibility that AA is generated by PLC and DAG lipase, and that downstream generation of PGE_2 (or EETs, see below) dilates the arterioles provided that NO suppresses 20-HETE formation.

The lack of dependence of arteriole dilation on astrocyte $[Ca^{2+}]_i$ changes contrasts with earlier work[1,2] in which mGluR agonists or Ca^{2+}-uncaging evoked arteriole dilation by raising astrocyte $[Ca^{2+}]_i$. We assume this relates to the different kinds of stimuli applied: release of endogenous neurotransmitter glutamate from synapses in this paper, versus the generation of a more spatially extensive $[Ca^{2+}]_i$ rise by bath superfusion of an mGluR agonist or essentially simultaneous Ca^{2+}-uncaging in several astrocytes. Consequently we cannot exclude the possibility that with other stimulation paradigms (or in other brain regions) mGluR-driven astrocyte Ca^{2+} signalling may contribute to arteriole dilation, although this mechanism may decrease in importance with age[15].

Overall, our data indicate that two cellularly- and chemically-distinct Ca^{2+}-dependent pathways mediate neurovascular coupling in response to neuronal activity evoked glutamate release (Supp. Fig. 1): ATP-evoked signalling in astrocytes generates PGE_2 which dilates capillaries via pericytes, and glutamate-evoked NO release from interneurons dilates arterioles. Previous data[6] suggest that the astrocyte-capillary pathway is faster, and quantitatively more important for increasing blood flow, than the interneuron-arteriole pathway, so our current data imply that purinergic signalling contributes significantly to generating BOLD signals.

We observed a similar block of capillary dilation after astrocyte Ca^{2+} buffering (64% reduction: Fig. 2c) and inhibition of $P2X_1$ receptors (58% reduction: Fig. 2l). The incomplete nature of this block (compared to that produced by inhibiting PLD2: Fig. 5k) may reflect an insufficient concentration of BAPTA or NF449 being applied. Alternatively, another mechanism might generate the remaining fraction of the response. We have ruled out direct signalling from neurons to pericytes via NMDA receptor mediated NO release[30] (Fig. 1e, h

and 4i, l), but other signals or Ca^{2+}-independent (e.g. cyclic nucleotide) mechanisms in astrocytes could be involved.

Previous reports have suggested that astrocyte-mediated neurovascular signalling involves AA metabolites, and our data demonstrate that this is true for signalling to capillaries. Conceivably EETs may contribute to neurovascular signalling to arterioles under some conditions[9,46,47], as we detected epoxygenase expression in astrocyte endfeet along larger vessels (but not in endfeet along capillaries (Supp. Fig. 5c) and EETs do not contribute to capillary dilation (Fig. 4c, f)[6]). Although AA production has been attributed to the activity of Ca^{2+}-dependent[48] PLA_2[2,8], which is expressed in astrocytes[33] (Supp. Fig. 6), we found that PLA_2 is not involved in neurovascular coupling. Instead, another Ca^{2+}-dependent phospholipase, PLD2, was responsible for AA production (Fig. 5h, k; Supp. Fig. 8c, d). In the brain, PLD1 may be expressed primarily in neurons or oligodendrocytes and PLD2 in astrocytes[34,49]. Furthermore, studies of the two PLD isoforms have suggested that PLD1 is expressed in endosomal compartments, depending on Ca^{2+} release from internal stores for activation, whereas PLD2 tends to be membrane associated and is activated by Ca^{2+} entry through ion channels[34,35]. Our findings suggest that astrocytic PLD2 is activated by Ca^{2+} entry through $P2X_1$ channels, which fits neatly with these data.

In conclusion, neuronal activity results in capillary dilation in a manner that is largely dependent on Ca^{2+}-dependent signalling in astrocytes. The astrocyte $[Ca^{2+}]_i$ rise causing dilation depends on ionotropic $P2X_1$ receptor activation, but not on GPCRs or TRPA1 channels. AA synthesis via a PLD2-DAGL pathway, and downstream metabolism into prostaglandin E_2 by COX1, are necessary for capillary dilation, with the required synthetic enzymes being expressed in astrocytes. In contrast, neuronally-evoked arteriole dilation depends at least partly on the activation of neuronal NMDA receptors and subsequent synthesis and release of NO. These data demonstrate that astrocytes are important contributors to neurovascular coupling at the capillary level and suggest that capillaries, which contain most of the resistance to blood flow in the brain parenchyma[50], could be specifically targeted therapeutically to increase blood flow in pathological conditions.

Accession codes: Not applicable

Data availability statement: The data that support the findings of this study are available from the corresponding author upon request.

Acknowledgements: Supported by the European Research Council (BRAINPOWER to D.A. and NETSIGNAL to D.R.), a Fondation Leducq Transatlantic Network grant (to D.A.), a Wellcome Trust Programme Grant and Senior Investigator Award (075232 and 099222 to D.A.), a Wellcome Trust Senior Research Fellowship (095064 and 200893 to A.V.G.), a Wellcome Trust Principal Research Fellowship (101896 to D.R.), an EU FP7 grant (ITN EXTRABRAIN 606950 to D.R.) and an RSF grant (15-14-30000 to D.R.). We thank K. Zheng for help with 2-photon microscopy, and M. Carandini, I. Christie, S. Cockcroft, M. Ford, R. Jolivet, S. Mastitskaya and S. Sullivan for comments on the manuscript.

Author contributions:

A.M. and D.A. conceived the study. A.M. carried out all brain slice experiments, some immunocytochemistry, and analysed brain slice and *in vivo* data; J.P.R. performed *in vivo* experiments and analysed the resulting data; Y.C. carried out immunocytochemistry; A.V.G. and D.A.R. provided *in vivo* expertise; A.M. and D.A. wrote the paper; all authors revised the paper.

References

1. Zonta, M.*, et al.* Neuron-to-astrocyte signaling is central to the dynamic control of brain microcirculation. *Nat. Neurosci.* **6**, 43-50 (2003).
2. Mulligan, S.J. & Macvicar, B.A. Calcium transients in astrocyte endfeet cause cerebrovascular constrictions. *Nature* **431**, 195-199 (2004).
3. Takano, T.*, et al.* Astrocyte-mediated control of cerebral blood flow. *Nat. Neurosci.* **9**, 260-267 (2006).
4. Zimmermann, K.W. Der Feinere Bau der Blutcapillaren. *Zeitschrift fur Anatomie und Entwicklungsgeschichte* **68**, 29-109 (1923).
5. Peppiatt, C.M., Howarth, C., Mobbs, P. & Attwell, D. Bidirectional control of CNS capillary diameter by pericytes. *Nature* **443**, 700-704 (2006).
6. Hall, C.N.*, et al.* Capillary pericytes regulate cerebral blood flow in health and disease. *Nature* **508**, 55-60 (2014).
7. Hamel, E. Perivascular nerves and the regulation of cerebrovascular tone. *J. Appl. Physiol.* **100**, 1059-1064 (2006).
8. Attwell, D.*, et al.* Glial and neuronal control of brain blood flow. *Nature* **468**, 232-243 (2010).
9. Mishra, A., Hamid, A. & Newman, E.A. Oxygen modulation of neurovascular coupling in the retina. *Proc. Natl. Acad. Sci. U.S.A.* **108**, 17827-17831 (2011).
10. Nizar, K.*, et al.* In vivo stimulus-induced vasodilation occurs without IP_3 receptor activation and may precede astrocytic calcium increase. *J. Neurosci.* **33**, 8411-8422 (2013).
11. Winship, I.R., Plaa, N. & Murphy, T.H. Rapid astrocyte calcium signals correlate with neuronal activity and onset of the hemodynamic response in vivo. *J. Neurosci.* **27**, 6268-6272 (2007).
12. Reeves, A.M., Shigetomi, E. & Khakh, B.S. Bulk loading of calcium indicator dyes to study astrocyte physiology: key limitations and improvements using morphological maps. *J. Neurosci.* **31**, 9353-9358 (2011).

13. Lind, B.L., Brazhe, A.R., Jessen, S.B., Tan, F.C. & Lauritzen, M.J. Rapid stimulus-evoked astrocyte Ca^{2+} elevations and hemodynamic responses in mouse somatosensory cortex in vivo. *Proc. Natl. Acad. Sci. U.S.A.* **110**, E4678-E4687 (2013).
14. Otsu, Y.*, et al.* Calcium dynamics in astrocyte processes during neurovascular coupling. *Nat. Neurosci.* **18**, 210-218 (2015).
15. Sun, W.*, et al.* Glutamate-dependent neuroglial calcium signaling differs between young and adult brain. *Science* **339**, 197-200 (2013).
16. Bonder, D.E. & McCarthy, K.D. Astrocytic Gq-GPCR-linked IP_3R-dependent Ca^{2+} signaling does not mediate neurovascular coupling in mouse visual cortex in vivo. *J. Neurosci.* **34**, 13139-13150 (2014).
17. Seifert, G. & Steinhauser, C. Glial cells in the mouse hippocampus express AMPA receptors with an intermediate Ca2+ permeability. *Eur. J. Neurosci.* **7**, 1872-1881 (1995).
18. Lalo, U., Pankratov, Y., Kirchhoff, F., North, R.A. & Verkhratsky, A. NMDA receptors mediate neuron-to-glia signaling in mouse cortical astrocytes. *J. Neurosci.* **26**, 2673-2683 (2006).
19. Lalo, U.*, et al.* $P2X_1$ and $P2X_5$ subunits form the functional P2X receptor in mouse cortical astrocytes. *J. Neurosci.* **28**, 5473-5480 (2008).
20. Shigetomi, E., Jackson-Weaver, O., Huckstepp, R.T., O'Dell, T.J. & Khakh, B.S. TRPA1 channels are regulators of astrocyte basal calcium levels and long-term potentiation via constitutive D-serine release. *J. Neurosci.* **33**, 10143-10153 (2013).
21. Gordon, G.R., Choi, H.B., Rungta, R.L., Ellis-Davies, G.C. & Macvicar, B.A. Brain metabolism dictates the polarity of astrocyte control over arterioles. *Nature* **456**, 745-749 (2008).
22. Mishra, A.*, et al.* Imaging pericytes and capillary diameter in brain slices and isolated retinae. *Nat. Protoc.* **9**, 323-336 (2014).
23. Panatier, A. & Robitaille, R. Astrocytic mGluR5 and the tripartite synapse. *Neuroscience* (2015).

24. Butt, A.M. ATP: a ubiquitous gliotransmitter integrating neuron-glial networks. *Semin. Cell Dev. Biol.* **22**, 205-213 (2011).
25. Haustein, M.D.*, et al.* Conditions and constraints for astrocyte calcium signaling in the hippocampal mossy fiber pathway. *Neuron* **82**, 413-429 (2014).
26. North, R.A. Molecular physiology of P2X receptors. *Physiol. Rev.* **82**, 1013-1067 (2002).
27. Shigetomi, E.*, et al.* Imaging calcium microdomains within entire astrocyte territories and endfeet with GCaMPs expressed using adeno-associated viruses. *J. Gen. Physiol.* **141**, 633-647 (2013).
28. Panatier, A.*, et al.* Astrocytes are endogenous regulators of basal transmission at central synapses. *Cell* **146**, 785-798 (2011).
29. Di Castro, M.A.*, et al.* Local Ca^{2+} detection and modulation of synaptic release by astrocytes. *Nat. Neurosci* **14**, 1276-1284 (2011).
30. Meng, W., Tobin, J.R. & Busija, D.W. Glutamate-induced cerebral vasodilation is mediated by nitric oxide through N-methyl-D-aspartate receptors. *Stroke* **26**, 857-862 (1995).
31. Stobart, J.L., Lu, L., Anderson, H.D., Mori, H. & Andersona C.M. Astrocyte-induced cortical vasodilation is mediated by D-serine and endothelial nitric oxide synthase. *Proc. Natl. Acad. Sci. U.S.A.* **110**, 3149-3154 (2013)..
32. Alkayed, N.J.*, et al.* Molecular characterization of an arachidonic acid epoxygenase in rat brain astrocytes. *Stroke* **27**, 971-979 (1996).
33. Stephenson, D.T.*, et al.* Calcium-sensitive cytosolic phospholipase A_2 ($cPLA_2$) is expressed in human brain astrocytes. *Brain. Res.* **637**, 97-105 (1994).
34. Cockcroft, S. Signalling roles of mammalian phospholipase D1 and D2. *Cell. Mol. Life Sci.* **58**, 1674-1687 (2001).
35. Sarri, E., Pardo, R., Fensome-Green, A. & Cockcroft, S. Endogenous phospholipase D2 localizes to the plasma membrane of RBL-2H3 mast cells and can be distinguished from ADP ribosylation factor-stimulated phospholipase D1 activity by its specific sensitivity to oleic acid. *Biochem. J.* **369**, 319-329 (2003).

36. Yemisci, M., *et al.* Pericyte contraction induced by oxidative-nitrative stress impairs capillary reflow despite successful opening of an occluded cerebral artery. *Nat. Med.* **15**, 1031-1037 (2009).

37. Duffy, S. & Macvicar, B. A. Adrenergic calcium signaling in astrocyte networks within the hippocampal slice. *J. Neurosci.* **15**, 5535-5550 (1995).

38. Calcinaghi, N., *et al.* Metabotropic glutamate receptor mGluR5 is not involved in the early hemodynamic response. *J. Cereb. Blood Flow Metab.* **31**, e1-10 (2011).

39. Srinivasan, R., *et al.* Ca^{2+} signaling in astrocytes from *Ip3r2*$^{-/-}$ mice in brain slices and during startle responses in vivo. *Nat. Neurosci.* **18**, 708-717 (2015).

40. Wells, J. A., *et al.* A critical role for purinergic signalling in the mechanisms underlying generation of BOLD fMRI responses. *J. Neurosci.* **35**, 5284-5292 (2015).

41. Wieraszko, A., Goldsmith, G. & Seyfried, T. N. Stimulation-dependent release of adenosine triphosphate from hippocampal slices. *Brain Res.* **485**, 244-250 (1989).

42. Zhang, Y. et al. An RNA-Seq transcriptome and splicing database of glia, neurons, and vascular cells of the cerebral cortex. *J. Neurosci.* **34**, 11929-11947 (2014).

43. Tricoire, L. & Vitalis, T. Neuronal nitric oxide synthase expressing neurons: a journey from birth to neuronal circuits. *Front. Neural Circuits* **6**, 82 (2012).

44. Schmidt, H.H., Pollock, J.S., Nakane, M., Förstermann, U., & Murad, F. Ca^{2+}/calmodulin-regulated nitric oxide synthase. *Cell Calcium* **13**, 427-434 (1992).

45. Lindauer, U., Megow, D., Matsuda, H., & Dirnagl, U. Nitric oxide: a modulator, but not a mediator, of neurovascular coupling in rat somatosensory cortex. *Am. J. Physiol. Heart Circ. Physiol.* **277**, H799-H811 (1999).

46. Metea, M. R. & Newman, E. A. Glial cells dilate and constrict blood vessels: a mechanism of neurovascular coupling. *J. Neurosci.* **26**, 2862-2870 (2006).

47. Lecrux, C., Kocharyan, A., Sandoe, C. H., Tong, X. K. & Hamel, E. Pyramidal cells and cytochrome P450 epoxygenase products in the neurovascular coupling response to basal forebrain cholinergic input. *J. Cereb. Blood Flow Metab.* **32**, 896-906 (2012).

48. Farooqui, A. A., Yang, H. C., Rosenberger, T. A. & Horrocks, L. A. Phospholipase A2 and its role in brain tissue. *J. Neurochem.* **69**, 889-901 (1997).
49. Zhang, Y.*, et al.* Increased expression of two phospholipase D isoforms during experimentally induced hippocampal mossy fiber outgrowth. *Glia* **46**, 74-83 (2004).
50. Blinder, P.*, et al.* The cortical angiome: an interconnected vascular network with noncolumnar patterns of blood flow. *Nature Neurosci.* **16**, 889-897 (2013).

Methods

Animals. Sprague-Dawley rats of both sexes were used in all experiments. Animal procedures were carried out in accordance with the guidelines of the UK Animals (Scientific Procedures) Act 1986 and European Directive 2010/63/EU. Each experiment was conducted on brain slices from at least three animals (at least one of each sex).

Brain slice preparation. As described previously[22], 300 μm thick coronal cortical slices were prepared from P21 rats on a vibratome in ice-cold oxygenated (95% O_2, 5% CO_2) solution containing (in mM) 93 N-methyl-D-glucamine chloride, 2.5 KCl, 30 $NaHCO_3$, 10 $MgCl_2$, 1.2 NaH_2PO_4, 25 glucose, 0.5 $CaCl_2$, 20 HEPES, 5 Na ascorbate, 3 Na pyruvate and 1 kynurenic acid. The slices were incubated at 34°C in the same solution for 15-20 min, then transferred to a similar solution with the NMDG-Cl, $MgCl_2$ and $CaCl_2$ replaced by (mM) 93 NaCl, 1 $MgCl_2$ and 2 $CaCl_2$, and incubated at room temperature (21–23°C) until used in experiments.

Imaging of capillaries in brain slices. Slices were perfused with bicarbonate buffered aCSF containing (in mM) 124 NaCl, 2.5 KCl, 26 $NaHCO_3$, 1 $MgCl_2$, 2 $CaCl_2$, 1 NaH_2PO_4, 10 glucose, 1 Na-ascorbate heated to 31-35°C and gassed with 20% O_2, 5% CO_2 and 75% N_2. Capillaries were imaged using differential interference contrast (DIC) microsopy at 20-50 μm depth within layers III-VI of cortical slices containing the motor and prefrontal cortices, using a 40x water immersion objective, a Coolsnap HQ2 CCD camera, and ImagePro Plus acquisition software. Images were acquired every 5 s, with an exposure time of 100 ms. The pixel size was 160 nm. The thromboxane A_2 analogue U46619 (200 nM) was used to preconstrict capillaries in all experiments where the vessel response to stimulation was evaluated. Although the cerebral cortex is highly vascularized, the slicing procedure leaves many vessels unhealthy and unable to actively respond to stimuli[22]. We only analyzed vessels that preconstricted to U46619, in order to ensure that the vessels used in our experiments were healthy and responsive. Vessel internal diameters were measured by manually placing a measurement line perpendicular to the vessel (Fig. 1a) on the image at locations where constriction to U46619 occurred (presumed regions of active pericyte

control) using Metamorph software. Change in diameter was quantified as a 30 s average centred around the largest response seen after stimulation, normalized to the baseline diameter. Experiments in which changes in focus occurred were excluded from further analysis. Data in the presence of blockers of signalling pathways were compared with interleaved control data obtained without the blockers to avoid confounds due to day-to-day variability in stimulation-evoked capillary responses. Control and drug experiments were randomly interleaved. To reduce experimenter bias, experiments were conducted and analyzed blind when possible (i.e. all experiments except when the drug was colored, e.g. NBQX).

Stimulation protocol for brain slices. High frequency (100 Hz) trains of short duration (200 ms [30-90 volt, 0.2 ms]), medium duration (the short stimulation repeated once per sec for 5 sec) or long duration (the short stimulation repeated once per sec for 1 minute) were applied using an aCSF-filled patch-pipette electrode placed 400-500 µm away from the imaged vessel. All stimulation durations evoked a capillary dilation with the same pharmacology (blocked by NF449: see Suppl. Fig. 3). All arteriole experiments were conducted using the 5 s medium duration stimulation. To confirm activation of the neurons, the field potential was monitored near the capillary of interest using a 4 MΩ patch pipette filled with aCSF (Supp. Fig. 2a, b), and only experiments where a field potential was detected were used for analysis. When characterizing field potentials in detail (Supp. Fig. 2), a 25 s long 12 Hz stimulation was used and the peak EPSC amplitude between 5 and 9 ms after stimulation was measured.

Pharmacology in brain slices. For all experiments, except those using L-161,982 and PPOH, vessels were preconstricted with U46619 which acts on thromboxane A_2 receptors (unpublished data kindly provided by Ben Barres, similar to those at http://web.stanford.edu/group/barres_lab/brain_rnaseq.html, show that pericytes express this receptor). The drug of interest was then bath applied for at least 5 minutes before stimulation-evoked capillary responses were evaluated. For L-161,982 experiments, slices were treated with L-161,982 for 5 minutes before preconstriction was achieved with U46619

(applied for 5 min) and stimulation-evoked dilations were then evaluated. This allowed us to confirm that PGE_2 signalling via EP_4 does not contribute to baseline capillary tone (constricted by 3.3±3.0%; p=0.3). Slices were incubated in PPOH for at least 1 hour before experiments and PPOH was included in all solutions (control and U46619-containing aCSF) to ensure that epoxygenase activity was blocked during stimulation experiments. A list of the drugs used is given in Supp. Table 1, along with the concentration and timeframe on which they have previously been shown to act.

α,β-methylene ATP puff experiments. A 5 s puff of external solution containing α,β-methylene ATP (100 μM) was used to activate $P2X_1$ receptors. ATP can constrict retinal pericytes and arterioles directly[5,51] and here we found the same effect when α,β-methylene ATP was bath applied to cortical slices (8.4±2.7% constriction, n=5). To avoid these direct effects of α,β-meATP on the vessel, the puff pipette was positioned 100-150 μm downstream (with respect to the perfusion flow) from the capillary of interest, with the aim of activating astrocytes at that location which would then signal to the imaged vessel. Lack of spread of the puffed solution to the imaged vessel was confirmed by including a dye in the puffing pipette on some occasions (Supp. Fig. 10).

Whole-cell patch-clamping of astrocytes. Slices were superfused with bicarbonate-buffered solution as described above, bubbled with 20% O_2, 5% CO_2 and 75% N_2, and heated to 33-36°C. Astrocytes were identified as cells with a soma of small diameter (~10 μm) that was not perfectly round. In some cases, slices were incubated at a very low concentration of Rhod-2 AM (4 μM), which loads relatively selectively into astrocytes and NG2-positive oligodendrocyte precursor cells. Astrocytes were whole-cell clamped at -80 mV with 3-5 MΩ patch pipettes with different internal solutions depending on the experiment being carried out. The control internal solution contained (in mM) 125 K-gluconate, 2 NaCl, 0.1 $CaCl_2$, 10 HEPES, 1 K_4-EGTA, 2 $MgCl_2$, 2 Na_2ATP, 0.5 Na_2GTP, 10 Na_2-phosphocreatine and 0.04 Alexa Fluor 488, with pH set to 7.1 using KOH. The internal solution containing BAPTA (tetra-potassium salt) was similar but with the $CaCl_2$ and EGTA replaced with (in mM) 3 $CaCl_2$ and 30 BAPTA (so that the free $[Ca^{2+}]_i$ was ~24.5 nM in both

the control and the BAPTA internal solutions, calculated using MaxChelator, Stanford) and with osmolarity differences compensated by lowering the K-gluconate concentration. Osmolarity measurements showed that K_4-BAPTA does not dissociate completely so that correspondingly less compensation of osmolarity was needed. The solution contained (mM) 67 K-gluconate, 2 NaCl, 3 $CaCl_2$, 10 HEPES, 30 K_4-BAPTA, 2 $MgCl_2$, 2 Na_2ATP, 0.5 Na_2GTP, 10 Na_2 phosphocreatine and 0.04 Alexa Fluor 488, with pH set to 7.1 using KOH. Patch-clamped cells were confirmed to be astrocytes morphologically by their arborization pattern revealed by dye filling and electrically by their large negative resting membrane potential (-91.6±0.6 mV, n=33), low input resistance (4.6±0.6 MΩ) and passive I-V relationship.

Calcium imaging of astrocytes. All neuronally-evoked astrocyte $[Ca^{2+}]_i$ imaging was carried out by confocal microscopy using a Zeiss LSM700 microscope. The internal solution used for Ca^{2+} imaging was similar to the control internal, but with added 50 μM Fluo-4 to sense Ca^{2+} and 40 μM Alexa 594 as a reference dye to allow ratiometric imaging, and $CaCl_2$ increased to 0.105 mM. The intensities of Fluo4 and Alexa 594 were measured using GECIquant[39] in a region of interest (ROI), and a background intensity measured far from the filled astrocyte at each time point was subtracted from the value in the ROI at the same time point. Data were quantified as fractional changes in the ratio of background-subtracted Fluo4 fluorescence to Alexa 594 fluorescence. Images were acquired at 0.4 Hz.

Immunohistochemistry. 200 μm thick coronal cortical slices were incubated in aCSF bubbled with 95% O_2 and 5% CO_2 containing 1 μM isolectin B_4 conjugated to Alexa 488 (which binds to α-D-galactose residues in the vascular basement membrane[52]) for 30 minutes to label vessels, then washed with aCSF and fixed in 4% paraformaldehyde for 1 hour. Slices were then washed 3 times in phosphate-buffered saline (PBS) and incubated in a blocking solution (comprised of 0.05% Triton X-100, 10% horse serum and 1% bovine serum albumin prepared in PBS for 1 hr) at room temperature. Slices were incubated with the primary antibody for 48-72 hrs at 4°C with agitation, washed 3 times with PBS, incubated with the secondary antibody overnight at 4°C with agitation and washed again 3 times with

PBS. The primary and secondary antibody solutions were prepared in PBS containing 0.005% Triton X-100, 1% horse serum and 0.1% bovine serum albumin. Controls to test for non-specific labeling of the secondary antibody were carried out in exactly the same manner, except that slices were incubated in just the vehicle (PBS containing 0.005% Triton X-100, 1% horse serum and 0.1% bovine serum albumin) during the primary antibody incubation step. The slices were then mounted with VectaShield hard set mounting medium containing DAPI to label nuclei. Immunohistochemistry experiments were conducted on three separate occasions on tissue from three different animals. Primary antibodies used were: chicken GFAP (Abcam, ab4674, 1:1000), rabbit AQP_4 (Santa Cruz, sc-20812, 1:500) or goat AQP_4 (Santa Cruz, sc-9888, 1:500), goat COX1 (Abcam, ab22720, 1:1000), goat COX2 (Abcam, ab23672, 1:1000), goat PGES (Santa Cruz, sc-12268, 1:500), rabbit PLD1 (Santa Cruz, sc-25512, 1:300), rabbit PLD2 (Santa Cruz, sc-25513, 1:200), mouse PLA_2 (Santa Cruz, sc-454, 1:300) and rabbit CYP2C11 (Abcam, ab3571, 1:300). Secondary antibodies used were: donkey anti-chicken Alexa 644 (Molecular Probes, 1:1000), donkey anti-chicken Cy5 (Jackson Laboratories, 1:1000), donkey anti-rabbit Alexa 647 (Molecular probes, 1:1000), donkey anti-goat Alexa 568 (Molecular probes, 1:1000), donkey anti-rabbit Alexa 555 (Molecular Probes, 1:1000) and donkey anti-mouse Cy3 (Jackson Immunoresearch Laboratories, 1:500). Immunolabelled slices were imaged using a Zeiss LSM700 confocal microscope.

***In vivo* experiments: preparation.** Experiments were conducted in male Sprague-Dawley rats (4 to 6 weeks of age). Animals were initially anaesthetised using isoflurane (5% induction, 2% maintenance). The femoral artery was cannulated for continuous blood pressure recording, as well as periodic blood gas monitoring. Following cannulation, a mixture of urethane (a single dose of 0.75 g/kg) and alpha-chloralose (an initial dose of 50 mg/kg supplemented with 10 mg/kg/hr) was administered intravenously while discontinuing isoflurane. Adequate anaesthesia was ensured by maintaining a stable arterial blood pressure and the absence of a withdrawal response to a paw pinch. The trachea was cannulated and the animal was mechanically ventilated during imaging sessions (1:2

oxygen/nitrogen ratio at 80 strokes min^{-1} and a tidal volume of 1 ml/100 g body weight). Body temperature was maintained at 37.0±0.5°C. The PO_2, PCO_2, and pH of the arterial blood were periodically measured using a RAPIDLab 348EX blood gas analyzer (Siemens), and the ventilation parameters were adjusted to keep these variables within their physiological ranges (PO_2 >80 mm Hg; PCO_2 30-45 mm Hg; and pH 7.35-7.45). Mean arterial blood pressure was stable at 90-110 mm Hg throughout the experiment. The animal was secured in a stereotaxic frame and a craniotomy of approximately 4 mm diameter was carried out over the right primary somatosensory cortex, immediately caudal to the coronal suture and approximately 2-6 mm laterally from the midline. A durectomy was subsequently performed. One microliter of the $P2X_1$ antagonist NF449 (5 μM) in artificial cerebrospinal fluid (aCSF; 124 mM NaCl, 3 mM KCl, 2 mM $CaCl_2$, 26 mM $NaHCO_3$, 1.25 mM NaH_2PO_4, 1 mM $MgSO_4$, 10 mM D-glucose saturated with 95% O2/5% CO2 [pH 7.4]), or one microliter of aCSF as a vehicle control, was pressure injected at 3-4 sites throughout the exposed cortical area, at a depth of 500 μm, using a glass micropipette. In order to distinguish cortical arterioles from venules and capillaries, Alexa 633 hydrazide[53] (35 μM, 1 μl) was included in the injection bolus. The cortical surface was covered with 0.8% agarose and a glass coverslip was placed on top. A custom built headplate was then attached to the skull and the entire assembly secured using dental cement. During imaging, the headplate was secured under the objective on a custom built stage.

***In vivo* experiments: imaging.** Cortical vessel diameter was recorded using 2P microscopy of the intraluminal dye fluorescein isothiocyanate-dextran (FITC-dextran, MW 2000 kDa, 50 mg/kg, 1 ml i.v.). Two-photon excitation was carried out using a Newport-Spectraphysics Ti:Sapphire MaiTai laser pulsing at 80 MHz, and an Olympus FV1000 with XLPlan N 25x water immersion objective (NA 1.05). Acquisitions were carried out using a wavelength of 800 nm and the mean laser power under the objective was kept at 20–30 mW. Penetrating arterioles were identified by chromatically separated Alexa 633 hydrazide fluorescent labelling of the smooth muscle elastin[53]. Recordings were made at a depth between 50 and 250 μm from the cortical surface. XY-time series (at 1–4 Hz with a pixel dwell time of 2 μs

and pixel size of 0.248-0.496 μm) were taken of regions of interest to record vessel dilations in response to somatosensory stimulation. Unilateral forepaw stimulation (0.3 ms pulse width, 3 Hz, 0.2-2 mA, 20 s) was applied using an electrical stimulator triggered by a 1401 interface (Cambridge Electronic Design).

***In vivo* experiments: analysis.** The presence of red blood cells (RBCs) leads to apparent holes in the images of the capillary and (to a lesser extent) the arteriole. This image noise was reduced by smoothing images in the time series with a rolling window (in time) maximum intensity projection not exceeding 2 s duration, as previously described[6]. The resulting time series was then median filtered (radius 1 pixel) using ImageJ. A 3-pixel wide line-segment was drawn perpendicular to the vessel in ImageJ and the fluorescence profile across the vessel was extracted. Relative diameter was determined by fitting a function to the fluorescence profile in Matlab (using the sum of 2 Gaussian functions), and calculating the full width at quarter-maximum of the peak fluorescence intensity. The peak dilation and the time to 10% of the peak dilation were calculated by fitting the data with a function of the form: $(max\ dilation).(time^n)/(time^n+K^n)$, with *max dilation*, *n* and *K* arbitrary constants

Statistics. Data are shown as box and whisker plots in which the central line shows the median, the central dot shows the mean, the edges of the box define the upper and lower quartile values, and the outer whiskers show the minimum-maximum range of the data, or are shown as mean±s.e.m. N numbers on bars are of capillary regions or arterioles. The variability of responses observed at different regions (presumed regions of active pericyte control) along the same capillary was higher than that between different capillaries, slices or animals. Therefore, capillary regions that constricted to 200 nM U46619 were used as the observational units. Normality of data was verified using the Kolmogorov-Smirnoff test and the equality of variance confirmed using the F-statistic. All data were compared to interleaved controls using a homoscedastic, two-sided Student's t-test (equal variance), except in Figs. 3c, 4j, 7f and Supp. Fig. 4d, where the variances of the data were unequal, and therefore a heteroscedastic, two-sided Student's t-test was used. Data in Supp. Fig. 2 were compared using a one-way ANOVA and corrected for multiple comparisons using a

procedure equivalent to the Holm-Bonferroni method (for N comparisons, the most significant p value is multiplied by N, the 2nd most significant by N-1, the 3rd most significant by N-2, etc.; corrected p values are significant if they are less than 0.05). An estimate of the sample size needed for a typical experiment is as follows: For a control response of 100%, a typical response standard deviation of 40%, a response in a drug of 30% (70% inhibition), a power of 80% and $p<0.05$, 7 vessels are needed (http://www.biomath.info/power/ttest.htm) in each of the control and drug groups. The exact numbers depend on the drug effect size and standard error of the data.

Materials. TTX, NBQX, D-AP5, S-MCPG, MRS2179 and A967079 were obtained from Tocris Biosciences; U46619, NF449, L-161982, U73122, CAY10441, PPOH, MAFP and FIPI from Cayman Chemicals; NS-398 and SC-560 from Calbiochem-Merck Millipore; RHC-80267 from Enzo Life Science; VU0155069 and CAY10594 from Santa Cruz; L-NNA, α,β-methylene ATP, NF023 and PGE_2 from Sigma; Alexa Fluor 488, Alexa Fluor 594, Fluo-4 pentapotassium salt, BAPTA tetrapotassium salt and Alexa Fluor 488 or FITC conjugated IB_4 from Life Technologies; and PBS and Alexa Fluor 633 hydrazide from Thermo Scientific. All other salts and reagents were purchased from Sigma.

Data Availability

The data that support the findings of this study are available from the corresponding author upon request.

Supplemental References

51. Kur, J. & Newman, E. A. Purinergic control of vascular tone in the retina. *J. Physiol.* **592**, 491-504 (2014).
52. Peters, B. P. & Goldstein, I. J. The use of fluorescein-conjugated Bandeiraea simplicifolia B4-isolectin as a histochemical reagent for the detection of alpha-D-galactopyranosyl groups. Their occurrence in basement membranes. *Exp. Cell Res.* **120**, 321-334 (1979).
53. Shen, Z., Lu, Z., Chhatbar, P. Y., O'Herron, P. & Kara, P. An artery-specific fluorescent dye for studying neurovascular coupling. *Nature Meth.* **9**, 273-276 (2012).
54. Nakatsuka, A., Mizuno, R., Ono, N., Nakayama, J. & Ohhashi, T. Arachidonic acid-induced COX-1 and COX-2-mediated vasodilation in rat gingival arterioles in vivo. *Jpn. J. Physiol.* **55**, 293-302 (2005).
55. Ito, S.*, et al.* Roles of stretch-activated cation channel and Rho-kinase in the spontaneous contraction of airway smooth muscle. *Eur. J. Pharmacol.* **552**, 135-142 (2006).
56. Wang, M. H.*, et al.* Cytochrome P450-derived arachidonic acid metabolism in the rat kidney: characterization of selective inhibitors. *J. Pharmacol. Exp. Ther.* **284**, 966-973 (1998).
57. Bley, K. R.*, et al.* RO1138452 and RO3244794: characterization of structurally distinct, potent and selective IP (prostacyclin) receptor antagonists. *Br. J. Pharmacol.* **147**, 335-345 (2006).
58. Myren, M., Olesen, J. & Gupta, S. Pharmacological and expression profile of the prostaglandin I(2) receptor in the rat craniovascular system. *Vascul. Pharmacol.* **55**, 50-58 (2011).
59. Shin, K. J.*, et al.* Phospholipase A_2-mediated Ca^{2+} influx by 2,2',4,6-tetrachlorobiphenyl in PC12 cells. *Toxicol. Appl. Pharmacol.* **178**, 37-43 (2002).

60. Smith, R. J., *et al.* Receptor-coupled signal transduction in human polymorphonuclear neutrophils: effects of a novel inhibitor of phospholipase C-dependent processes on cell responsiveness. *J. Pharmacol. Exp. Ther.* **253**, 688-697 (1990).
61. Su, W., *et al.* 5-Fluoro-2-indolyl des-chlorohalopemide (FIPI), a phospholipase D pharmacological inhibitor that alters cell spreading and inhibits chemotaxis. *Mol. Pharmacol.* **75**, 437-446 (2009).
62. Scott, S. A., *et al.* Design of isoform-selective phospholipase D inhibitors that modulate cancer cell invasiveness. *Nat. Chem. Biol.* **5**, 108-117 (2009).
63. Weigl, L., Zidar, A., Gscheidlinger, R., Karel, A. & Hohenegger, M. Store operated Ca^{2+} influx by selective depletion of ryanodine sensitive Ca^{2+} pools in primary human skeletal muscle cells. *Naunyn Schmiedebergs Arch. Pharmacol.* **367**, 353-363 (2003).
64. Rettinger, J., *et al.* Profiling at recombinant homomeric and heteromeric rat P2X receptors identifies the suramin analogue NF449 as a highly potent $P2X_1$ receptor antagonist. *Neuropharmacol.* **48**, 461-468 (2005).
65. Soto, F., Lambrecht, G., Nickel, P., Stuhmer, W. & Busch, A. E. Antagonistic properties of the suramin analogue NF023 at heterologously expressed P2X receptors. *Neuropharmacol.* **38**, 141-149 (1999).

Figure Legends

Figure 1. Neuronal activity evokes capillary dilation. (**a**) A cortical capillary response to 200 nM U46619 and superimposed neuronal stimulation (stim). Lines show lumen diameters plotted in b. (**b**) U46619 evoked constriction and stimulation-evoked dilation at regions indicated in a (in this and subsequent example traces, a large response is shown for illustrative purposes). (**c**) 500 nM TTX blocks stimulation-evoked capillary dilation. (**d**) 10 µM NBQX blocks stimulation-evoked dilation. (**e**) 25 µM D-AP5 did not reduce stimulation-evoked dilation. (**f-h**) Mean data showing the block of capillary dilation by TTX (**f**) and NBQX (**g**) but not by D-AP5 (**h**). Numbers on bars are capillary regions (putative pericytes) studied. Data are shown as box and whisker plots as defined in the Statistics part of the Methods.

Figure 2. $P2X_1$-evoked astrocyte Ca^{2+} signalling mediates capillary-level neurovascular coupling. (**a**) A DIC image of a cortical capillary (left panel) and the AlexaFluor 488 fill of the astrocyte network after whole-cell patch-clamp dialysis for 1 min (middle) and 10 mins (right) after breaking into the cell. Whole-cell patch-clamped cell is indicated by arrowhead and endfoot indicated by arrow. (**b**) Example traces and (**c**) mean data demonstrating that stimulation-evoked capillary dilation is intact when the astrocyte network is dialyzed with a control internal solution containing 1 mM EGTA but significantly reduced when filled with 30 mM BAPTA, a fast Ca^{2+}-chelator. (**d-f**) An inhibitor of group I and II mGluRs, S-MCPG (1 mM; **d**), the $P2Y_1$ blocker MRS2179 (25 µM; **e**) and the TRPA1 blocker A967079 (10 µM; **f**) do not block stimulation-evoked capillary dilation. (**g**) The $P2X_1$ blocker NF449 (100 nM) significantly reduced stimulation-evoked capillary dilation. (**h**) Puff-application of the $P2X_1$ agonist α,β-methylene ATP (α,β-meATP, 100 µM) to the neuropil downstream of the vessel induces capillary dilation. (**i-l**) Quantification of the effect of S-MCPG (**i**), MRS2179 (**j**), A967079 (**k**) and NF449 (**l**) on capillary dilation. (**m**) Mean response of capillaries in experiments like those in h, puffing external solution (control) or α,β-methylene ATP. Change in diameter in control experiments was measured as a 30 s average centred around

the largest response seen between 30 and 120 s after puff of α,β-methylene ATP. Data are shown as box and whisker plots as defined in the Statistics part of the Methods.

Figure 3. Neuronally-evoked astrocyte $[Ca^{2+}]_i$ rise depends on $P2X_1$ receptors. (**a**) An astrocyte patch-loaded with AlexaFluor 594 (top) and Fluo4 (bottom) showing the processes, endfoot and soma. White dashed lines delineate the vessel lumen ensheathed by the endfoot process. (**b**) Neuronal stimulation evoked a $[Ca^{2+}]_i$ rise in astrocyte endfeet in control conditions (left); the rise was smaller in the presence of the $P2X_1$ blocker NF449 (100 nM, right). Arrow indicates a spontaneous Ca^{2+} transient, demonstrating that Fluo-4 could still detect $[Ca^{2+}]_i$ transients with NF449 present. (**c**) Mean change in neuronally-evoked astrocyte $[Ca^{2+}]_i$ in somata, processes and endfeet in the absence and presence of different blockers. NF449 (black bars), a blocker of P2X1 channels, significantly reduced the $[Ca^{2+}]$ rise in processes and endfeet, but S-MCPG, a blocker of groups I and II mGluRs had no effect on astrocyte $[Ca^{2+}]$ in any compartment (grey bars). Time to 10% of the peak and to the peak $[Ca^{2+}]$ change in endfeet were 5.27±1.15 s and 11.57±2.39 s respectively. Data are shown as box and whisker plots as defined in the Statistics part of the Methods.

Figure 4. AA metabolites mediating stimulation-evoked capillary dilation. (**a**) The COX1 blocker SC-560 (1 μM) blocks the dilation. (**b,c**) The COX2 blocker NS-398 (10 μM; **b**) and the epoxygenase inhibitor PPOH (25 μM; **c**) had no effect on the dilation. (**d-f**) Mean data for the effect of SC-560 (**d**), NS-398 (**e**) and PPOH (**f**) on capillary dilation. (**g**) Blocking the PGE_2 receptor EP_4 with L-161,982 (1 μM) inhibits dilation. (**h,i**) Blocking the PGI_2 receptor IP with CAY10441 (1 μM; **h**) or NO synthase with L-NNA (100 μM; **i**) has no effect on capillary dilation. (**j-l**) Mean data showing that capillary dilation is blocked by L-161,982 (**j**), but not by CAY10441 (**k**) or L-NNA (**l**). Data are shown as box and whisker plots as defined in the Statistics part of the Methods.

Figure 5. PLD2, not PLA_2, initiates neurovascular coupling at the capillary level. (**a**) The PLA_2 inhibitor MAFP (10 μM) does not block stimulation-evoked capillary dilation. (**b**) The PLC blocker, U73122 (10 μM), does not reduce dilation. (**c**) The PLD blocker FIPI (1 μM) inhibits dilation. (**d-f**) Mean data showing the effects of MAFP (**d**), U73122 (**e**) and FIPI

(**f**) on capillary dilation. (**g**) Blocking PLD1 with VU0155069 (500 nM) had no effect on the dilation. (**h-i**) The PLD2 blocker CAY10594 (1 μM; **h**) and the DAGL blocker RHC80267 (50 μM; **i**) significantly reduce the capillary dilation. (**j-l**) Mean data showing the effect of VU0155069 (**j**), CAY10594 (**k**) and RHC80267 (**l**) on capillary dilation. Data are shown as box and whisker plots as defined in the Statistics part of the Methods.

Figure 6. Neurovascular signalling to arterioles is mediated by NMDAR and NOS activity, and not by astrocyte Ca^{2+}. (**a**) Example traces and (**b**) mean data demonstrating that stimulation-evoked arteriole dilation is not altered when the astrocyte network is dialyzed with 30 mM BAPTA, a fast Ca^{2+}-chelator, compared to a control internal solution containing 1 mM EGTA. (**c-e**) The $P2X_1$ blocker NF449 (100 nM; **c**), the PLA_2 inhibitor MAFP (10 μM; **d**) and the PLD2 blocker CAY10594 (1 μM; **e**) do not block stimulation-evoked arteriole dilation. (**f-g**) The NMDA receptor blocker D-AP5 (25 μM; **f**) and the NO synthase blocker L-NNA (100 μM; **g**) abolished the arteriole dilation. Mean data showing the effect of NF449 (**h**), MAFP (**i**), CAY10594 (**i**), D-AP5 (**j**) and L-NNA (**k**) on arteriole dilation. Data are shown as box and whisker plots as defined in the Statistics part of the Methods.

Figure 7. Neurovascular signalling to capillaries *in vivo* is mediated by $P2X_1$ receptors. (**a**) Two-photon stack (90 μm thick, maximum intensity projection) of FITC-dextran-filled vessels (green) in the somatosensory cortex of an anaesthetised rat. (**b**) Enlarged image showing a penetrating arteriole with a capillary branching off it. (**c-d**) Example traces of forepaw stimulation-evoked dilation of arterioles (**c**) and capillaries (**d**) in the presence of vehicle (aCSF, black traces) or the $P2X_1$ blocker NF449 (5 μM; red traces). Capillary dilations occurred faster than arteriole dilations (time to 10% dilation was 3.0±0.8s for 12 capillaries and 5.1±1.7s for 9 arterioles), as previously reported[6]; however, reflecting the smaller number of vessels studied, this effect did not reach significance in this study ($p=0.3$). (**e**) The percentage of arterioles (Art) and capillaries (Cap) that dilated in response to stimulation was not significantly different in NF449 and vehicle-treated animals. (**f**) Forepaw stimulation-evoked mean arteriolar dilation was similar in vehicle and NF449

treated animals, but capillary dilation was significantly inhibited by NF449. Data are shown as box and whisker plots as defined in the Statistics part of the Methods.

Supplementary Figure Legends

Supplementary Figure 1. Schematic diagram of the mechanisms underlying neurovascular signalling to capillaries and arterioles. Synaptic activity (top) evokes ATP release from post-synaptic neurons, which activates ionotropic ATP receptors containing $P2X_1$ subunits on astrocytes, leading to a rise in $[Ca^{2+}]_i$ via influx from the extracellular space. This rise in $[Ca^{2+}]_i$ activates PLD2, resulting in the formation of phosphatidic acid (PA) which is converted into diacylglycerol (DAG), which is then further metabolized by DAG lipase into arachidonic acid (AA). AA is then metabolized, by the consecutive activity of COX1 and PGES, to produce PGE_2, which dilates capillaries by acting on EP_4 receptors, presumably on pericytes. Synaptic activation of Ca^{2+} entry through NMDA receptors increases NOS activity in interneurons, resulting in NO release onto arterioles to dilate them. The neurovascular coupling pathways involved in signalling to capillaries and arterioles are highlighted in blue, while the enzymes and receptors ruled out by our experiments are shown in red with black crosses.

Supplementary Figure 2. Stimulation-evoked field potentials and identification of vessels. (**a-b**) A schematic (**a**) and a low-magnification image (**b**) of a cortical slice demonstrating the placement of the stimulation and recording electrodes. Cortical layers are indicated. Inset shows a high magnification image of the recording electrode near a capillary. (**c**) Stimulation-evoked fibre volley and field excitatory post-synaptic currents (fEPSCs) are not affected by U46619. NBQX blocks the fEPSCs but not the fibre volley and TTX blocks both the fibre volley and the fEPSCs. (**d**) Mean data (peak fEPSC amplitude measured 5 to 9 ms after the stimulation) showing the effect of U46619 and NBQX on fEPSCs. (**e**) Arterioles can be distinguished by the thick layer of smooth muscle cells (SMC, white brackets) that surround them, shown here alongside FITC-isolectin B_4 (IB_4) labeling of the basement membrane. (**f, g**) Capillaries are identified as smaller vessels that have only occasional pericyte cell bodies (arrowheads) outlined by the IB_4-labeling. IB_4 also labels microglia (asterisk). Vessel lumen is marked by red brackets. Data shown as mean±s.e.m.

Supplementary Figure 3. Constriction of cortical capillaries evoked by U46619 before each experiment. (**a**) Example trace of a U46619 (200 nM) induced capillary constriction lasting at least 30 minutes. (**b**-**x**) Mean constriction of capillaries to U46619 in interleaved control and drug experiments for the: (**b**) voltage-gated sodium channel blocker TTX, (**c**) AMPA/KA receptor blocker NBQX, (**d**) NMDA receptor blocker D-AP5, (**e**) fast Ca^{2+} chelator BAPTA, (**f**) inhibitor of group I and II mGluRs S-MCPG, (**g**) $P2Y_1$ blocker MRS2179, (**h**) TRPA1 blocker A967079, (**i**) $P2X_1$ blocker NF449, (**j**) $P2X_1$ blocker NF023, (**k**) COX1 blocker SC-560, (**l**) COX2 blocker NS-398, (**m**) epoxygenase blocker PPOH, (**n**) EP_4 receptor blocker L-161,982, (**o**) IP receptor blocker CAY10441, (**p**) NO synthase blocker L-NNA, (**q**) PLA_2 blocker MAFP, (**r**) PLC blocker U73122, (**s**) PLD blocker FIPI, (**t**) PLD1 blocker VU0155069, (**u**) PLD2 blocker CAY10594, (**v**) DAGL blocker RHC80267, (**w**) $P2X_1$ agonist α,β-meATP, and (**x**) PGE_2 in the presence or absence of the PLD blocker FIPI. P-values comparing U46619-evoked constrictions for control and drug experiments were >0.05 for all panels even without correcting for multiple comparisons. For experiments involving BAPTA (**e**), PPOH (**m**) and L-161,982 (**n**), U-46619 was applied in the presence of the relevant drug (see Methods). For all other experiments, vessels were pre-constricted with U46619 before drug application. Data shown as mean±s.e.m.

Supplementary Figure 4. Signalling to capillary pericytes is similar for different stimulation durations in P21 rats, and in P45 rats. Mean dilation (left panels) and time traces of the diameter change (right panels) observed in cortical capillaries following electrical stimulation of neuronal activity (at 100 Hz for 0.2 sec, repeated once/sec) in the absence and presence of $P2X_1$ blockers. (**a-c**) Capillary dilation evoked by short (200 ms; **a**), medium (5 sec; **b**) or long duration (1 min; **c**, reproduced from Fig. 2l) stimulation in slices from P21 rats is inhibited by the $P2X_1$ blocker NF449 (100 nM). (**d**) Stimulation-evoked capillary dilation in slices from P21 rats is inhibited by a second $P2X_1$ blocker NF023 (5 µM). (**e**) Stimulation-evoked capillary dilation in slices from P45 rats is also inhibited by the $P2X_1$ blocker NF449 (100 nM). Data shown as mean±s.e.m.

Supplementary Figure 5. COX1 and PGES are expressed in astrocyte endfeet along vessels. (**a**) AQP_4-expressing astrocyte endfeet along arterioles (arrows) and capillaries (arrowheads) are immunoreactive for COX1. Vascular basement membrane is labeled with Alexa dye conjugated isolectin B_4 (IB_4). (**b**) COX2 is absent from GFAP-expressing astrocyte somata (white asterisk) and endfeet (arrowhead) but is expressed in neuronal cell bodies (black asterisk). (**c**) Epoxygenase (CYP2C11) is expressed in AQP_4-expressing astrocyte endfeet along arterioles (arrows) but not in those along capillaries (arrowhead). Arterioles can be identified as larger vessels, often with space between layers of IB_4-labeled basement membrane (white circle) where the vascular smooth muscle cells are located. (**d**) PGES is expressed in GFAP-expressing astrocyte cell bodies (white asterisk), processes and endfeet along vessels (arrowheads). (**e**) Control experiments where slices were incubated with the secondary antibody used to stain the enzyme shown in the corresponding panels in a-d, but with the primary antibody omitted, demonstrating the lack of non-specific binding. Control for the secondary antibody used to detect COX1 is shown in the top row, COX2 in the second row, epoxygenase in third row and PGES in the fourth row.

Supplementary Figure 6. PLA_2 is expressed in GFAP-labeled astrocyte endfeet along the vasculature. Arrowhead indicates a pericyte cell body.

Supplementary Figure 7. PLD is upstream of PGE_2 in the signalling pathway. (**a**) After preconstriction with 200 nM U46619, applying 1 µM PGE_2 evokes a dilation. (**b**) A similar PGE_2-evoked dilation was seen in the presence of 1 µM FIPI to block PLD1 and PLD2. (**c**) Quantification of data from experiments like those in panels a-b, showing that PLD inhibition does not affect the capillary dilation evoked by PGE_2. Data shown as mean±s.e.m.

Supplementary Figure 8. PLD1 and PLD2 expression in the cortex. (**a, b**) PLD1 was diffusely expressed in the cortical neuropil and appeared concentrated in endothelial cells along arterioles (arrow, **a**) but not capillaries (**b**). No PLD1 labeling was observed in AQP_4-labeled endfeet (arrowheads). (**c, d**) PLD2 expression was detected in GFAP-expressing astrocyte endfeet along capillaries (arrowheads, **c**) as well as in astrocyte somata (asterisks, **d**). (**e**) Control experiments where slices were labeled with the secondary antibody used to

detect the enzymes shown in the corresponding panels in a-d, but with the primary antibody omitted, demonstrating the lack of non-specific binding. Control for secondary antibodies used to detect PLD1 is shown in the top two panels and for PLD2 is shown in the last two panels (for these pictures illumination was applied appropriate for evoking fluorescence from the secondary antibody used for PLD1/PLD2 labeling and from the dye-conjugated IB_4 or DAPI).

Supplementary Figure 9. Constriction of cortical arterioles evoked by U46619 before each experiment. Mean constriction of arterioles to U46619 in interleaved control and drug experiments for the: (**a**) $P2X_1$ blocker NF449, (**b**) PLA_2 blocker MAFP and PLD2 blocker CAY10594 (experiments were on the same animals with interleaved controls in common), (**c**) fast Ca^{2+} chelator BAPTA, (**d**) NMDA receptor blocker D-AP5, (**e**) NO synthase blocker L-NNA. P-values comparing U46619-evoked constrictions for control and drug experiments were >0.05 for all panels even without correction for multiple comparisons. Data shown as mean±s.e.m.

Supplementary Figure 10. Experimental set-up for puffing α,β-methylene ATP. (**a**) DIC image of slice showing a capillary. (**b**) DIC image of the slice surface showing position of the puff pipette. (**c**) Fluorescence image showing the pipette containing Alexa Fluor 594 positioned above the slice. (**d-i**) The spread of the Alexa Fluor 594 dye imaged at the start (**d**) and 5 consecutive seconds (**e-**i) following a 5 s puff at 5 psi. Note how the dye flows downwards and does not reach the location of the vessel at the top (demarcated by white dotted lines).

Supplementary Table 1. The concentration used, IC_{50}/K_i and timeframe of action reported previously for the blockers used in this study.

Drug	Blocker for	Working concentration	Selectivity	Concentration used	Shown to work within	Reference
SC-560	COX1	IC_{50}=9 nM	High, blocks COX2 with IC_{50} of 6 µM	1 µM	6 min	54
NS-398	COX2	IC_{50}=1.8 µM	High, blocks COX1 with IC_{50} of 75 µM	10 µM	2 min	55
PPOH	CYP450 Epoxygenase	IC_{50}=9 µM	Highly selective against CYP450 ω-hydroxylases	25 µM	30 min	56
L-161,982	PGE_2 receptor EP_4	K_i= 240 nM	Selective against prostaglandin receptors; K_i=0.7 µM for TxA_2 receptor	1 µM	5 min	6
CAY10441 (RO1138452)	PGI_2 receptor IP	IC_{50}=1.5 nM	Selective against COX and EP_{1-4} receptors	1 µM	2 min	57, 58
MAFP	PLA_2	IC_{50}=0.5 µM	Does not block PLC or PLD	10 µM	5 min	59
U73122	PLC	IC_{50}= 30 nM	Selective against phospholipases, may potentiate IP_3-mediated Ca^{2+} rise	10 µM	3 min	60
FIPI	PLD	IC_{50}= 25 nM (PLD1), 20 nM (PLD2)	Highly selective for PLD1 and PLD2	1 µM	5 min	61
VU0155069	PLD1	IC_{50}= 46 nM	IC_{50}=0.9 µM for PLD2	500 nM	5 min	62
CAY10594	PLD2	IC_{50}= 10 nM	IC_{50}=1-5 µM for PLD1	1 µM	5 min	62
RHC80267	DAG lipase	IC_{50}= 4 µM	Selective against PLA_2 and PLC	50 µM	2 min	63
NF449	$P2X_1$ receptors	IC_{50}=0.3 nM ($P2X_1$), 0.7 nM ($P2X_{1/5}$)	High, blocks $P2X_3$ with IC_{50} = 1 µM	100 nM	5 min	64
NF023	$P2X_1$ receptors	IC_{50}=0.24 µM	High, blocks $P2X_3$ with IC_{50} = 8.5 µM and $P2X_2$ at >50 µM	5 µM	Immediately	65

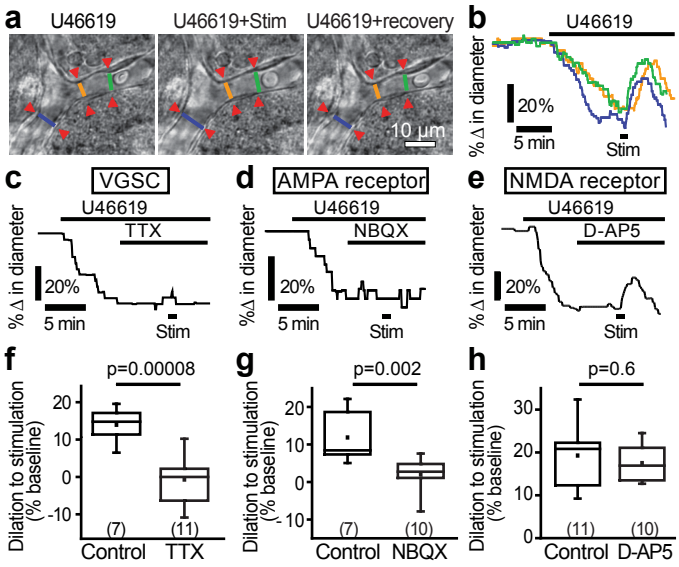
a
U46619
U46619+Stim
U46619+recovery
10 µm
b
U46619
% Δ in diameter
20%
5 min
Stim
c
VGSC
U46619
TTX
d
AMPA receptor
U46619
NBQX
e
NMDA receptor
U46619
D-AP5
f
p=0.00008
Dilation to stimulation (% baseline)
(7)
(11)
Control
TTX
g
p=0.002
(7)
(10)
Control
NBQX
h
p=0.6
(11)
(10)
Control
D-AP5

Figure 1

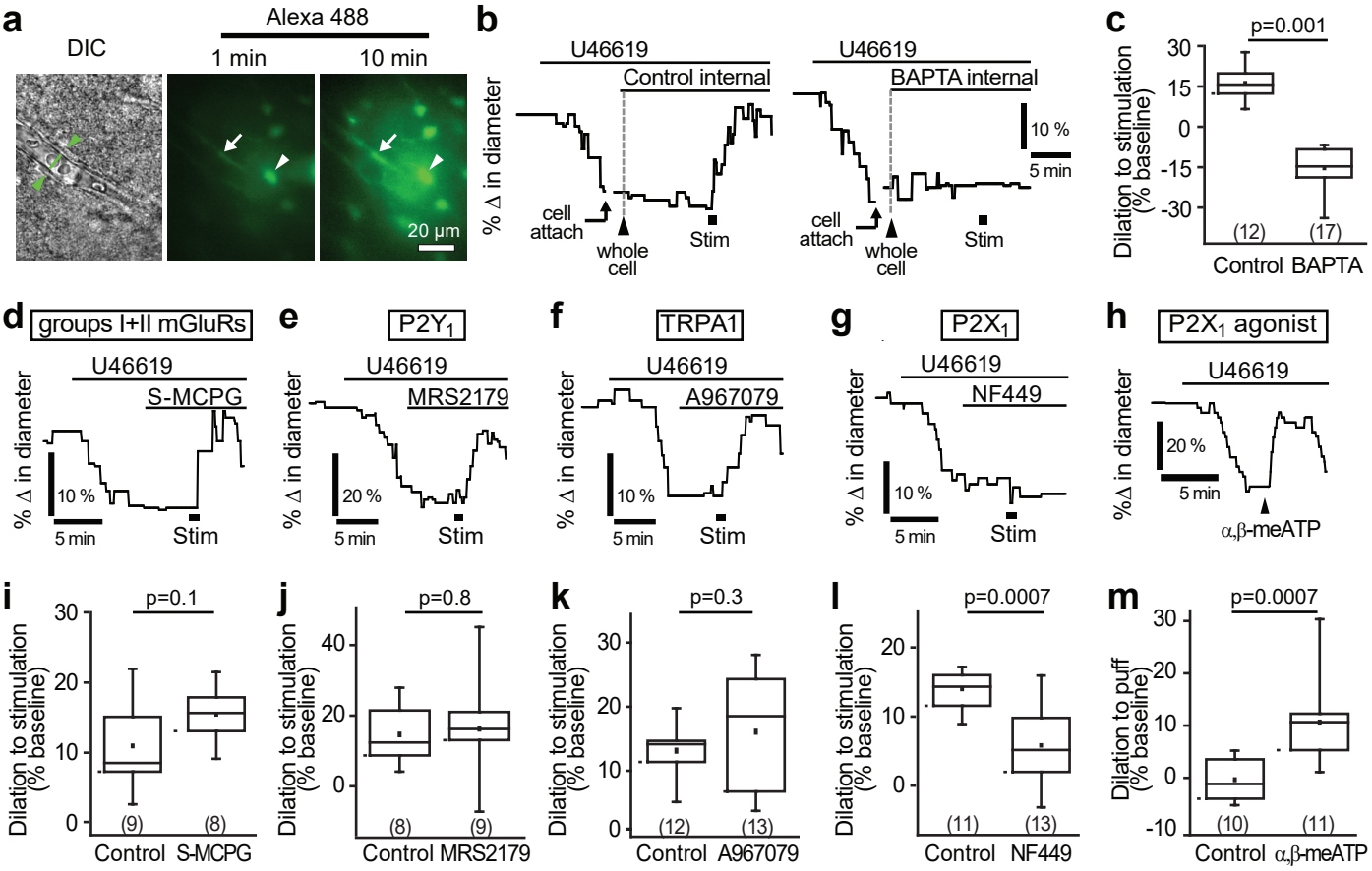
a
DIC
Alexa 488
1 min
10 min
20 µm
b
U46619
Control internal
BAPTA internal
% Δ in diameter
cell attach
whole cell
Stim
10 %
5 min
c
p=0.001
Dilation to stimulation (% baseline)
Control
BAPTA
(12)
(17)
d
groups I+II mGluRs
S-MCPG
e
P2Y1
MRS2179
f
TRPA1
A967079
g
P2X1
NF449
h
P2X1 agonist
α,β-meATP
i
p=0.1
Control
S-MCPG
(9)
(8)
j
p=0.8
Control
MRS2179
(8)
(9)
k
p=0.3
Control
A967079
(12)
(13)
l
p=0.0007
Control
NF449
(11)
(13)
m
p=0.0007
Dilation to puff (% baseline)
Control
α,β-meATP
(10)
(11)

Figure 2

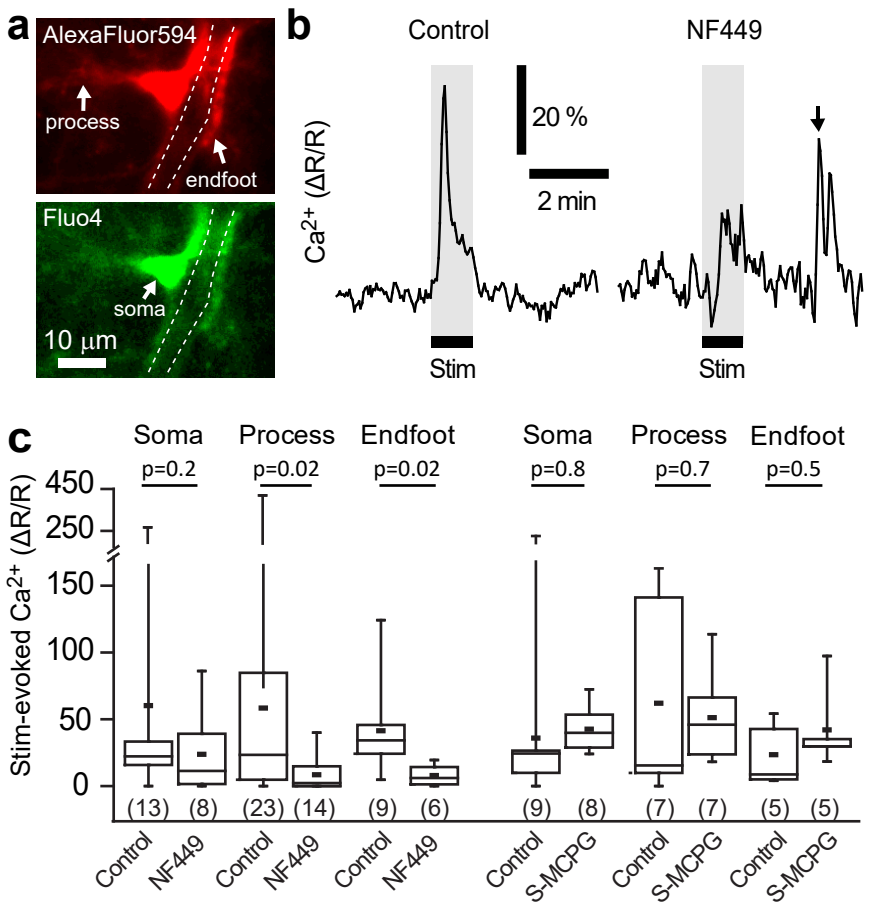
a
AlexaFluor594
process
endfoot
Fluo4
soma
10 µm
b
Control
NF449
20 %
2 min
Ca2+ (ΔR/R)
Stim
Stim
c
Soma
Process
Endfoot
Soma
Process
Endfoot
p=0.2
p=0.02
p=0.02
p=0.8
p=0.7
p=0.5
Stim-evoked Ca2+ (ΔR/R)
450
250
150
100
50
0
(13) (8) (23) (14) (9) (6) (9) (8) (7) (7) (5) (5)
Control
NF449
Control
NF449
Control
NF449
Control
S-MCPG
Control
S-MCPG
Control
S-MCPG

Figure 3

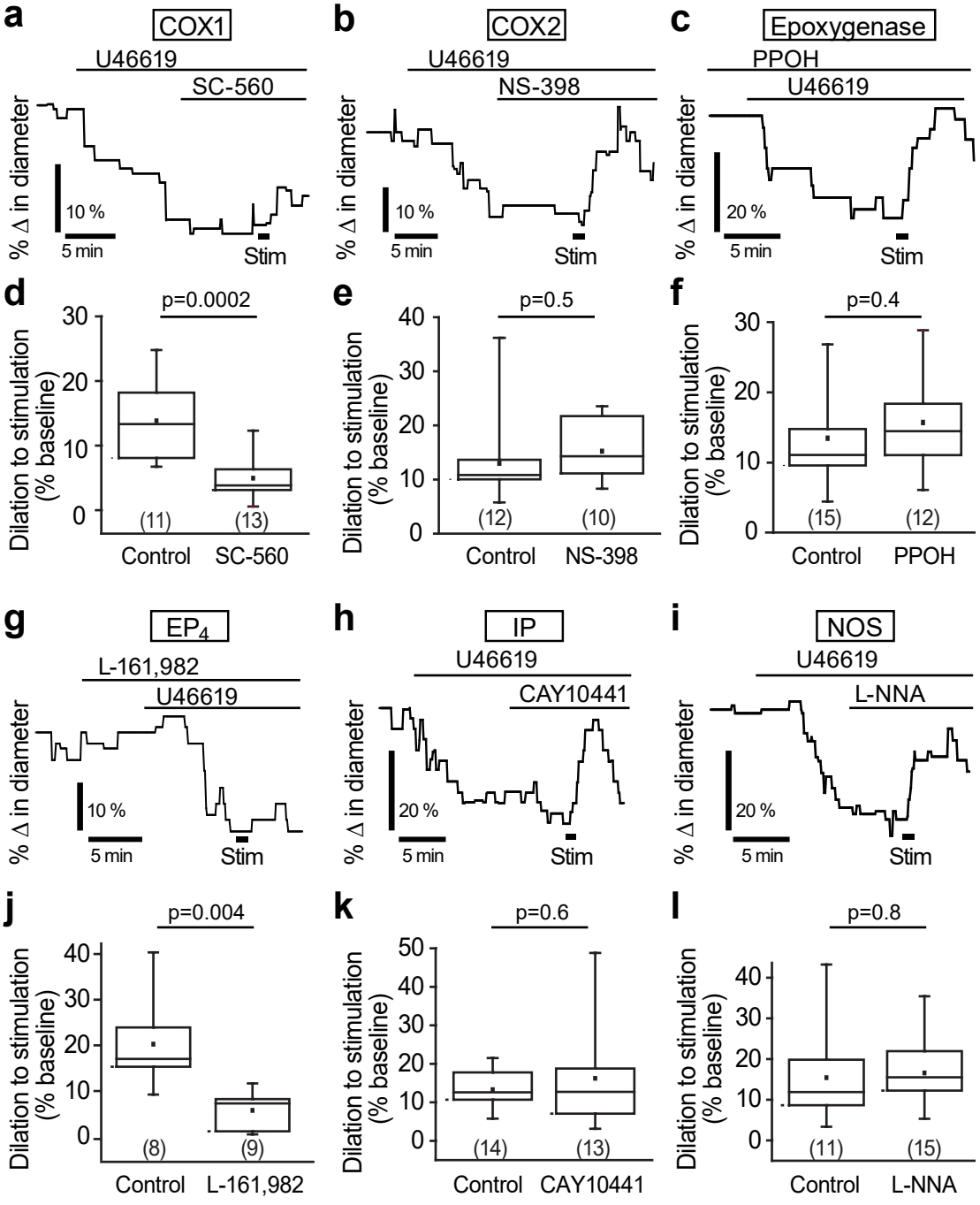
a
COX1
U46619
SC-560
% Δ in diameter
10 %
5 min
Stim
b
COX2
U46619
NS-398
% Δ in diameter
10 %
5 min
Stim
c
Epoxygenase
PPOH
U46619
% Δ in diameter
20 %
5 min
Stim
d
p=0.0002
Dilation to stimulation (% baseline)
30
20
10
0
(11)
(13)
Control
SC-560
e
p=0.5
Dilation to stimulation (% baseline)
40
30
20
10
0
(12)
(10)
Control
NS-398
f
p=0.4
Dilation to stimulation (% baseline)
30
20
10
0
(15)
(12)
Control
PPOH
g
EP4
L-161,982
U46619
% Δ in diameter
10 %
5 min
Stim
h
IP
U46619
CAY10441
% Δ in diameter
20 %
5 min
Stim
i
NOS
U46619
L-NNA
% Δ in diameter
20 %
5 min
Stim
j
p=0.004
Dilation to stimulation (% baseline)
40
30
20
10
0
(8)
(9)
Control
L-161,982
k
p=0.6
Dilation to stimulation (% baseline)
50
40
30
20
10
0
(14)
(13)
Control
CAY10441
l
p=0.8
Dilation to stimulation (% baseline)
40
30
20
10
0
(11)
(15)
Control
L-NNA

Figure 4

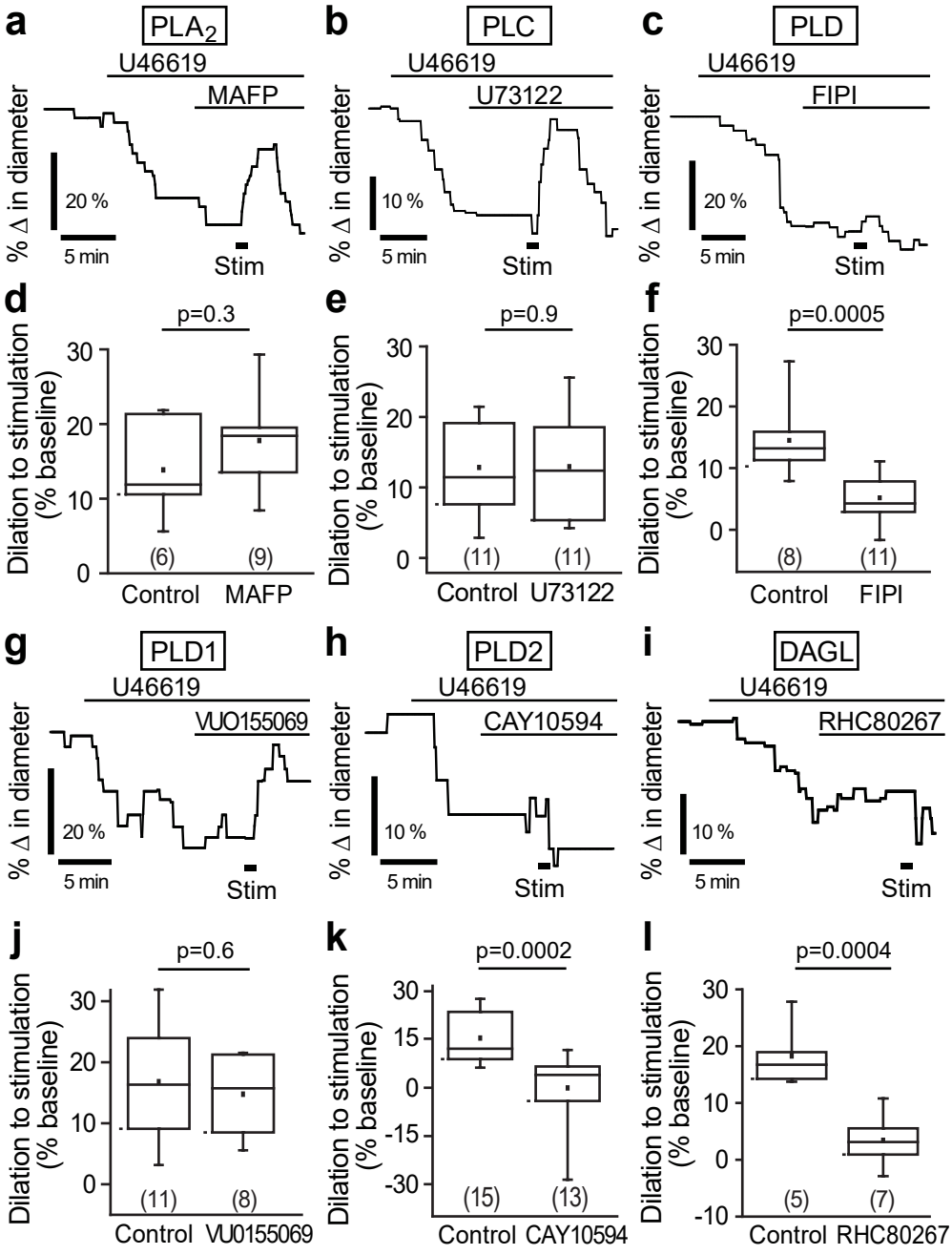
a
PLA2
U46619
MAFP
% Δ in diameter
20 %
5 min
Stim
b
PLC
U46619
U73122
% Δ in diameter
10 %
5 min
Stim
c
PLD
U46619
FIPI
% Δ in diameter
20 %
5 min
Stim
d
p=0.3
Dilation to stimulation (% baseline)
30
20
10
0
(6)
(9)
Control
MAFP
e
p=0.9
Dilation to stimulation (% baseline)
30
20
10
0
(11)
(11)
Control
U73122
f
p=0.0005
Dilation to stimulation (% baseline)
30
20
10
0
(8)
(11)
Control
FIPI
g
PLD1
U46619
VUO155069
% Δ in diameter
20 %
5 min
Stim
h
PLD2
U46619
CAY10594
% Δ in diameter
10 %
5 min
Stim
i
DAGL
U46619
RHC80267
% Δ in diameter
10 %
5 min
Stim
j
p=0.6
Dilation to stimulation (% baseline)
30
20
10
0
(11)
(8)
Control
VU0155069
k
p=0.0002
Dilation to stimulation (% baseline)
30
15
0
-15
-30
(15)
(13)
Control
CAY10594
l
p=0.0004
Dilation to stimulation (% baseline)
30
20
10
0
-10
(5)
(7)
Control
RHC80267

Figure 5

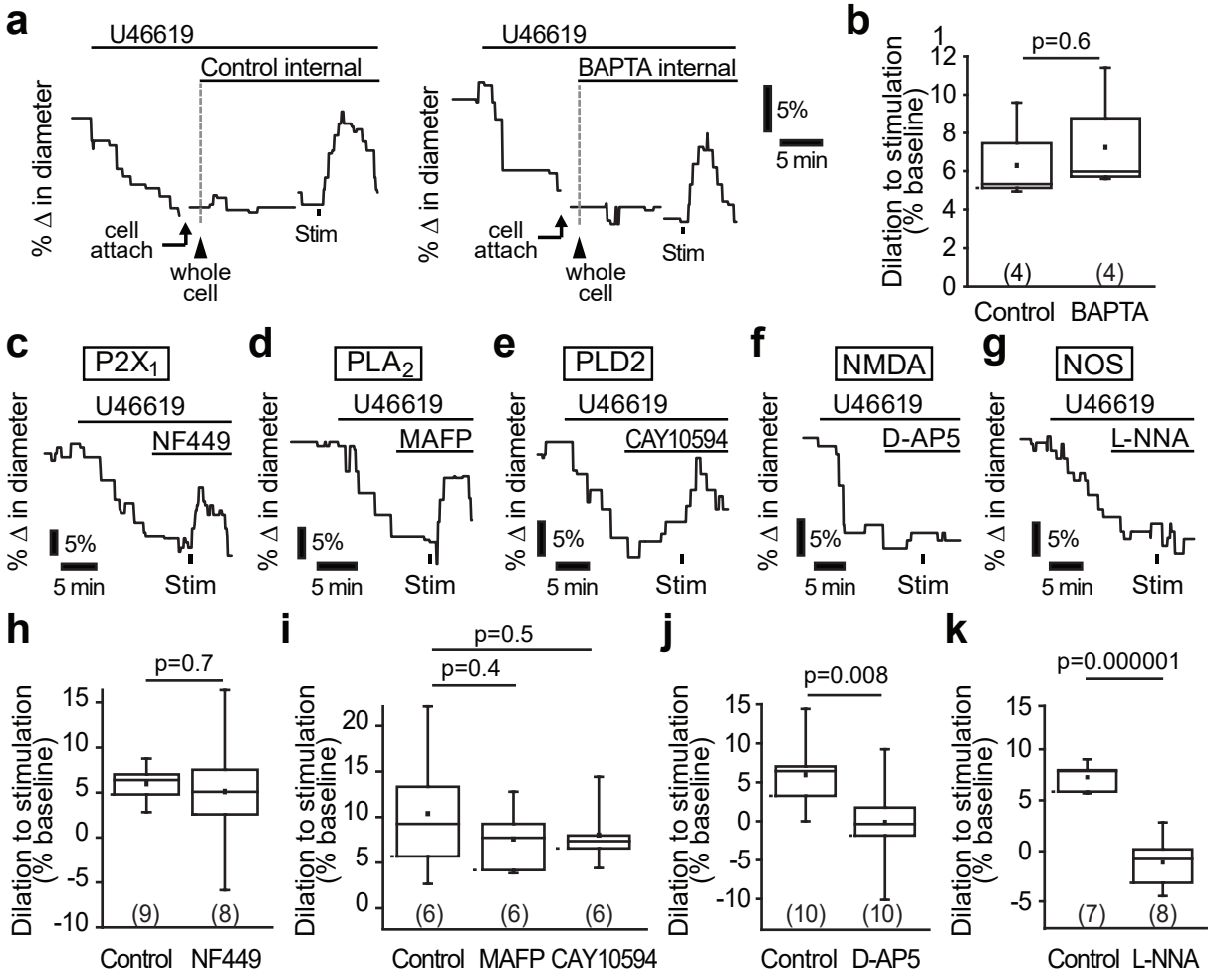
a
U46619
Control internal
% Δ in diameter
cell attach
whole cell
Stim
U46619
BAPTA internal
% Δ in diameter
cell attach
whole cell
Stim
5%
5 min
b
p=0.6
Dilation to stimulation (% baseline)
(4)
(4)
Control
BAPTA
c
P2X1
U46619
NF449
% Δ in diameter
5%
5 min
Stim
d
PLA2
U46619
MAFP
% Δ in diameter
5%
5 min
Stim
e
PLD2
U46619
CAY10594
% Δ in diameter
5%
5 min
Stim
f
NMDA
U46619
D-AP5
% Δ in diameter
5%
5 min
Stim
g
NOS
U46619
L-NNA
% Δ in diameter
5%
5 min
Stim
h
p=0.7
Dilation to stimulation (% baseline)
(9)
(8)
Control
NF449
i
p=0.5
p=0.4
Dilation to stimulation (% baseline)
(6)
(6)
(6)
Control
MAFP
CAY10594
j
p=0.008
Dilation to stimulation (% baseline)
(10)
(10)
Control
D-AP5
k
p=0.000001
Dilation to stimulation (% baseline)
(7)
(8)
Control
L-NNA

Figure 6

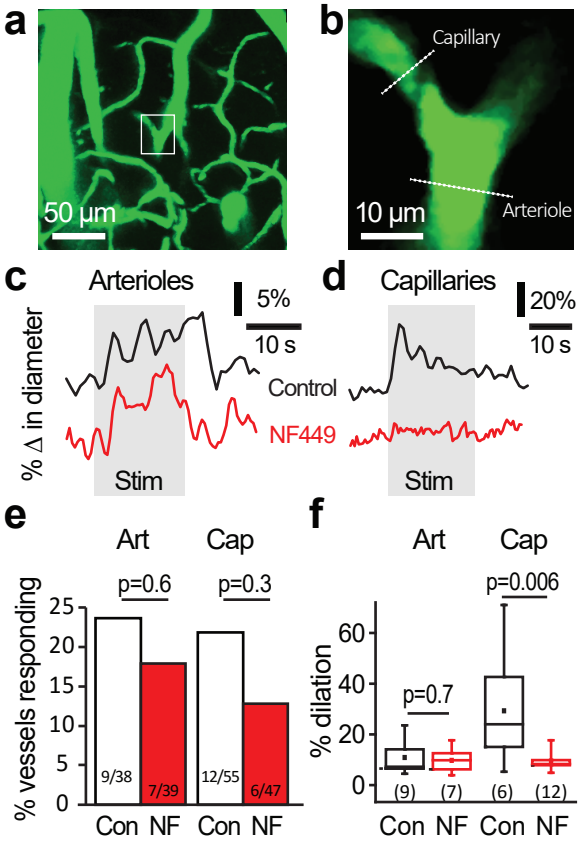
a
50 µm
b
Capillary
10 µm
Arteriole
c
Arterioles
5%
10 s
% Δ in diameter
Control
NF449
Stim
d
Capillaries
20%
10 s
Stim
e
Art
Cap
p=0.6
p=0.3
% vessels responding
25
20
15
10
5
0
9/38
7/39
12/55
6/47
Con NF Con NF
f
Art
Cap
p=0.006
p=0.7
% dilation
60
40
20
0
(9) (7) (6) (12)
Con NF Con NF

Figure 7

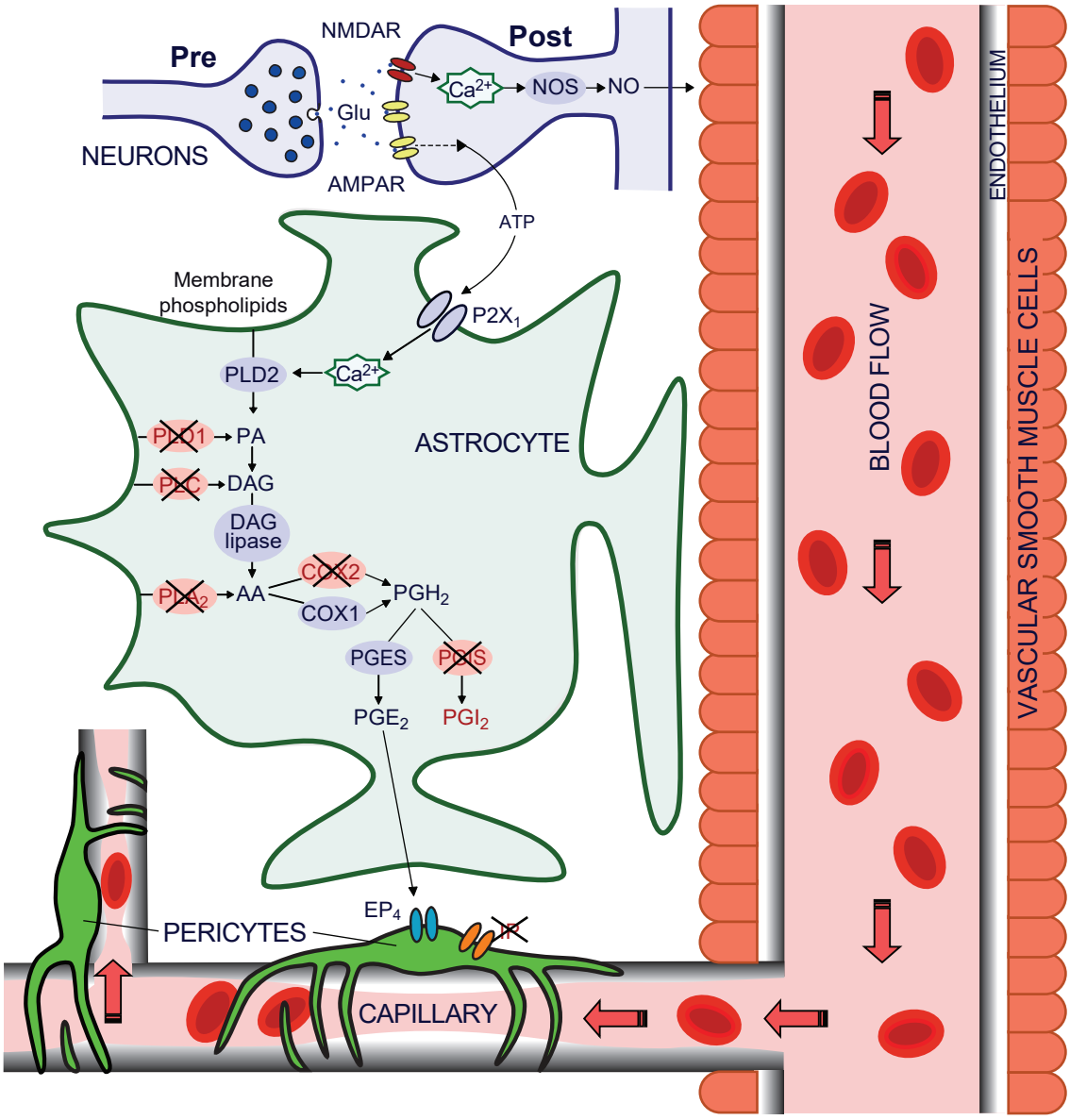

Supplementary Figure 1

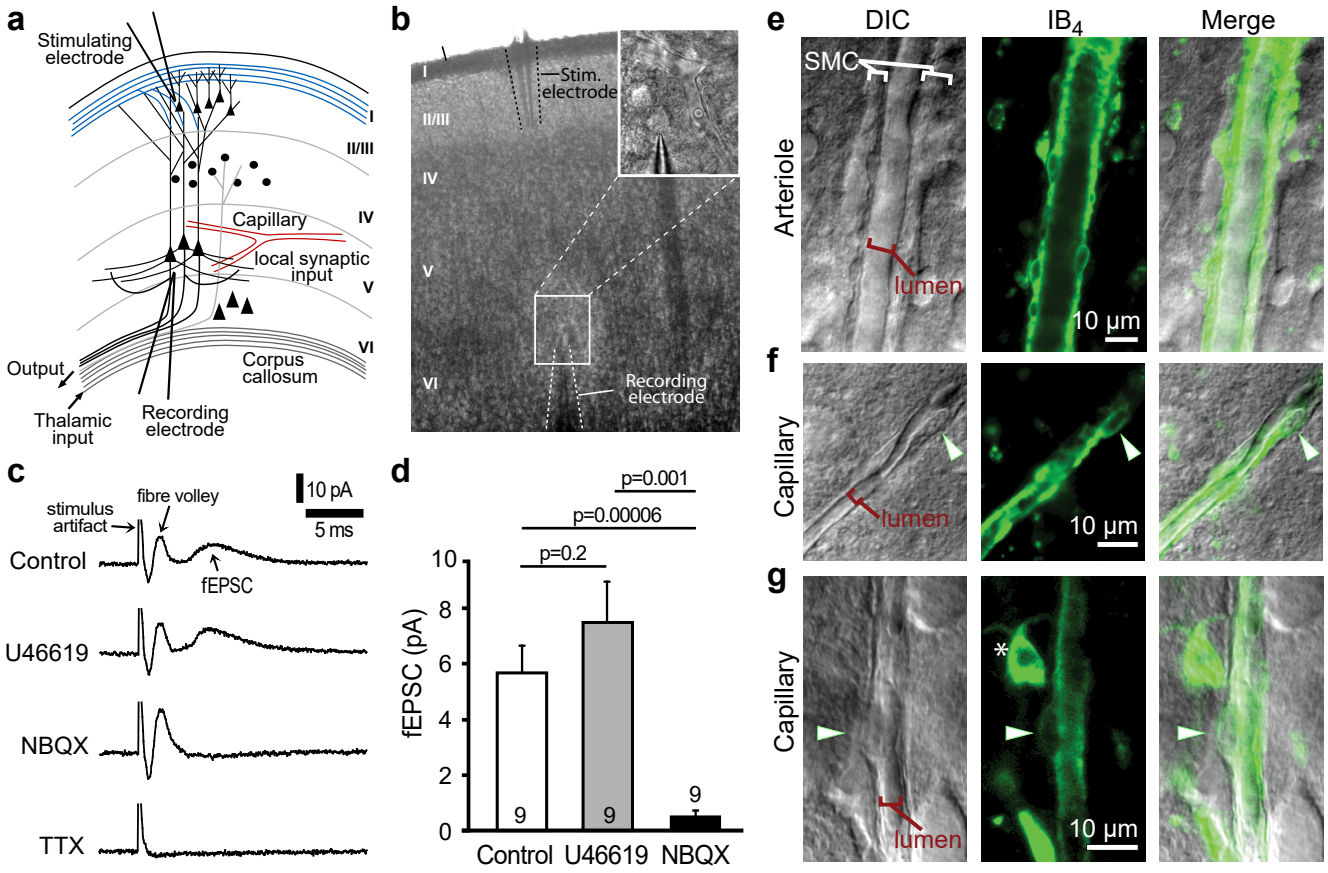

Supplementary Figure 2

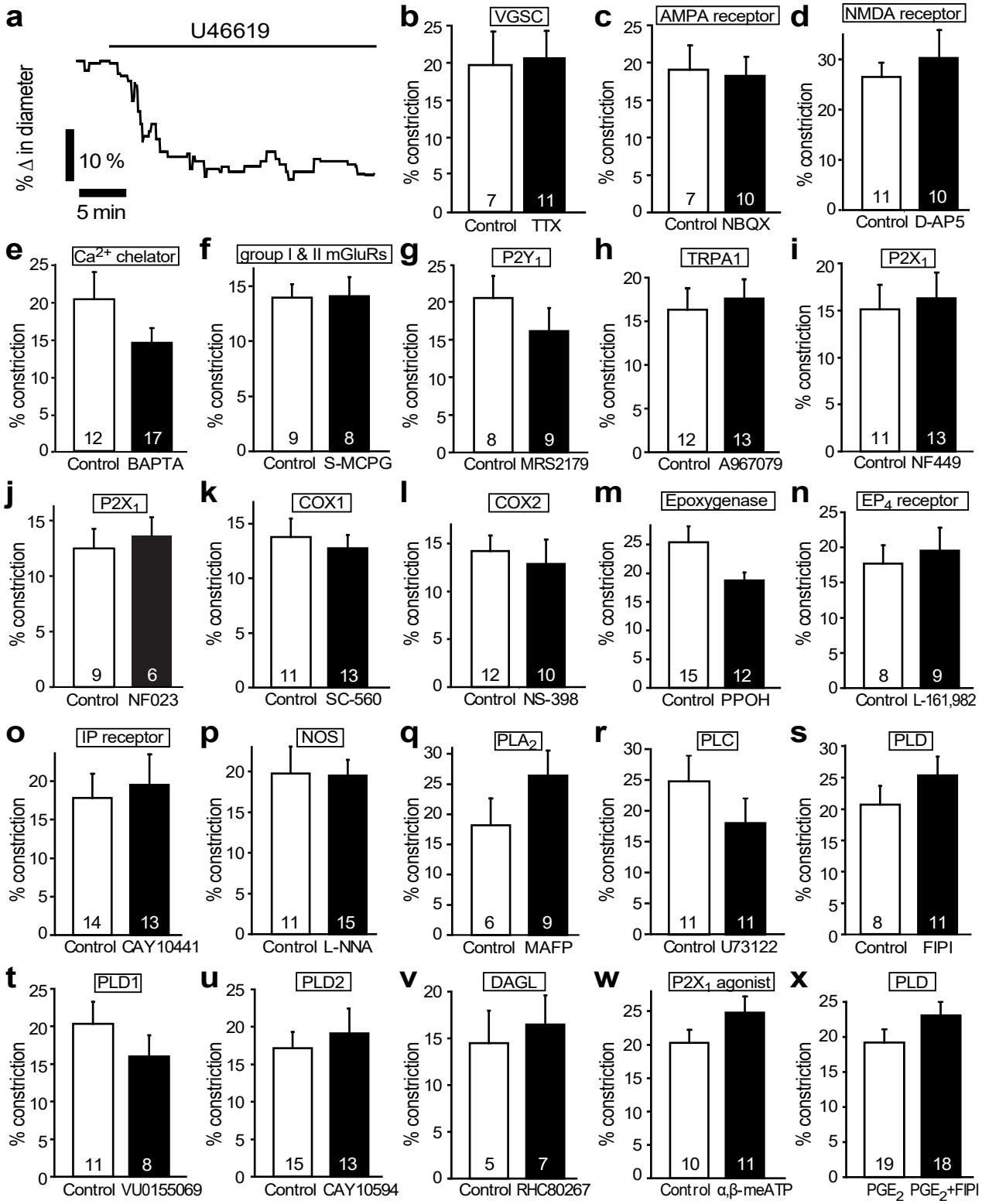

Supplementary Figure 3

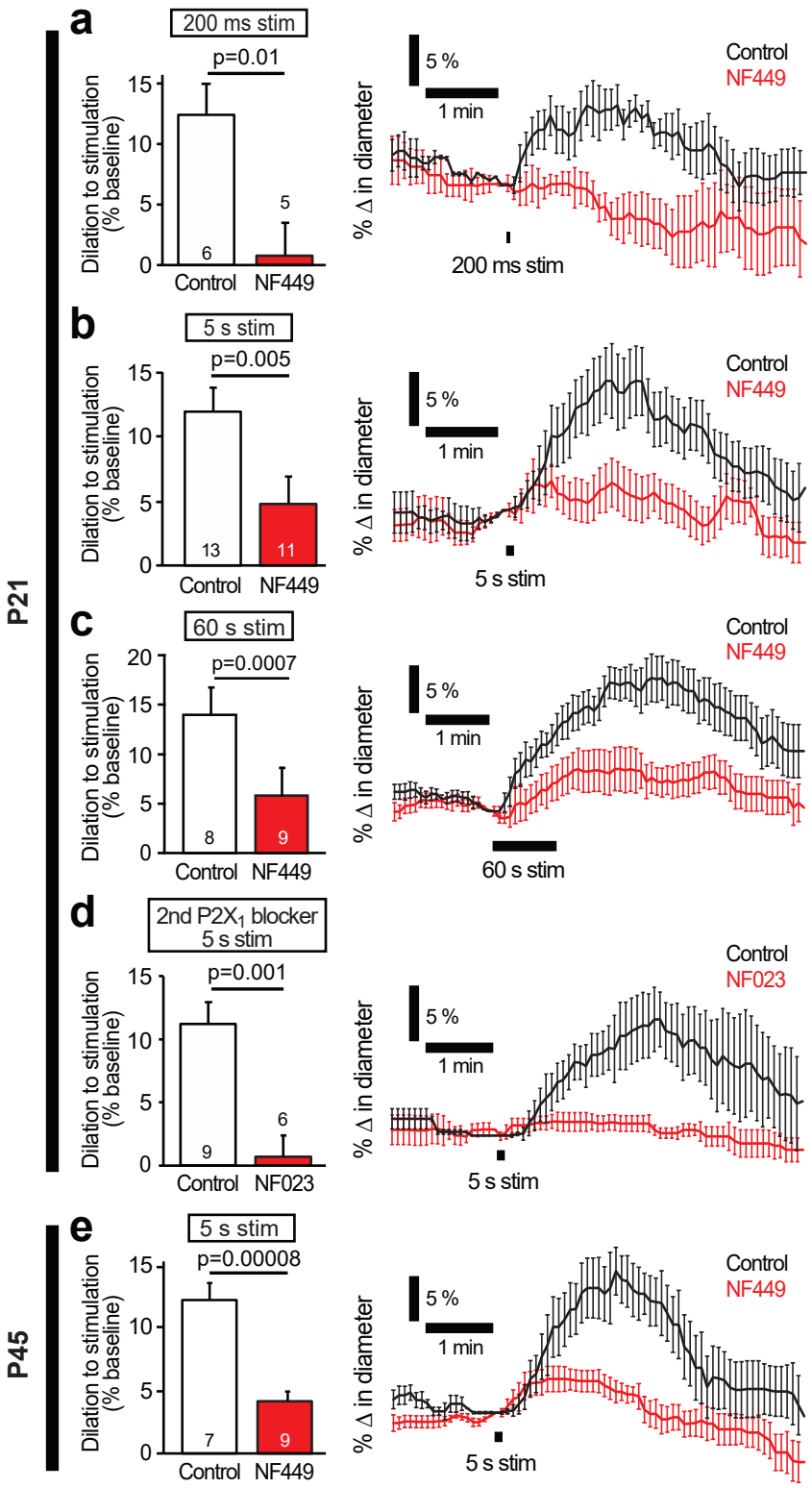

Supplementary Figure 4

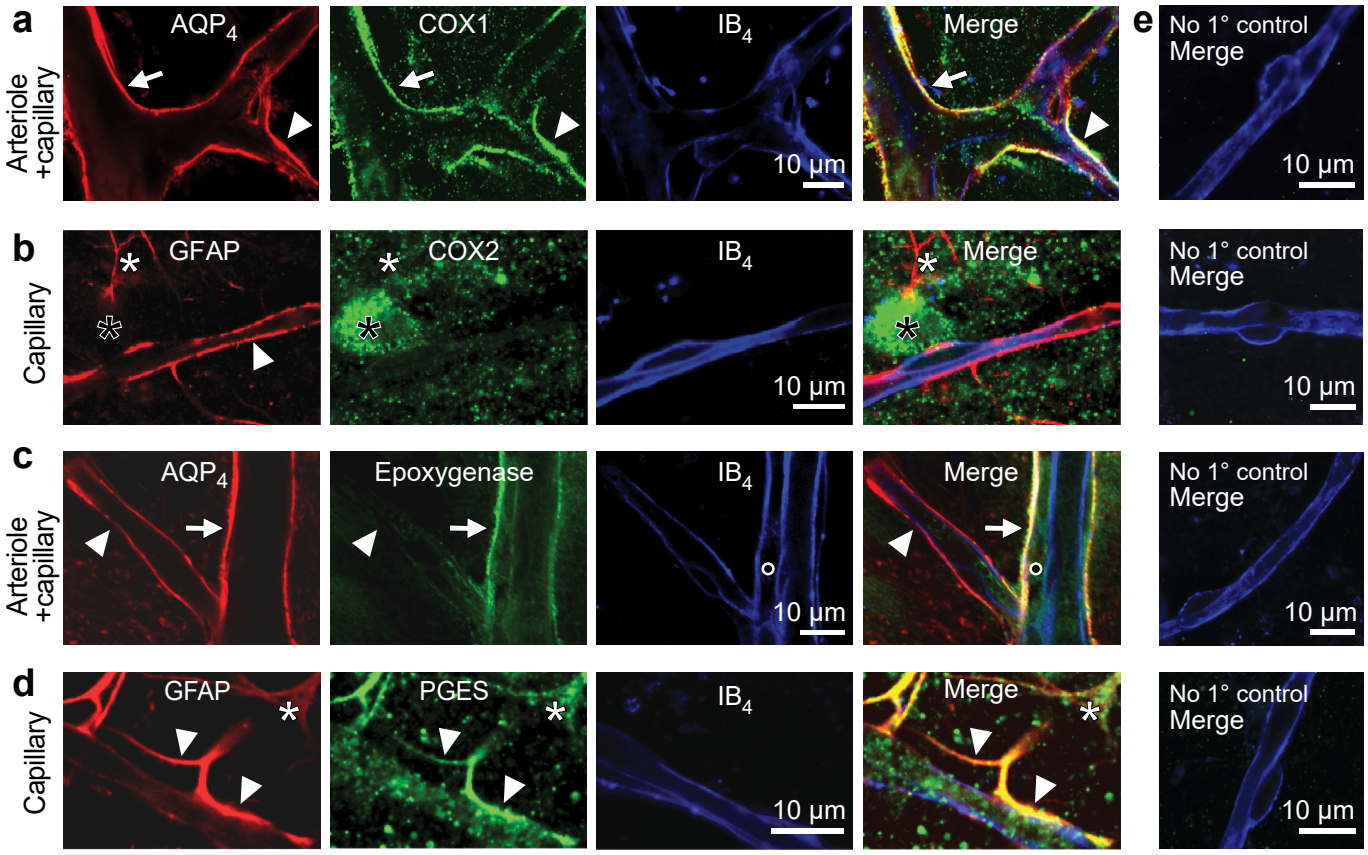

Supplementary Figure 5

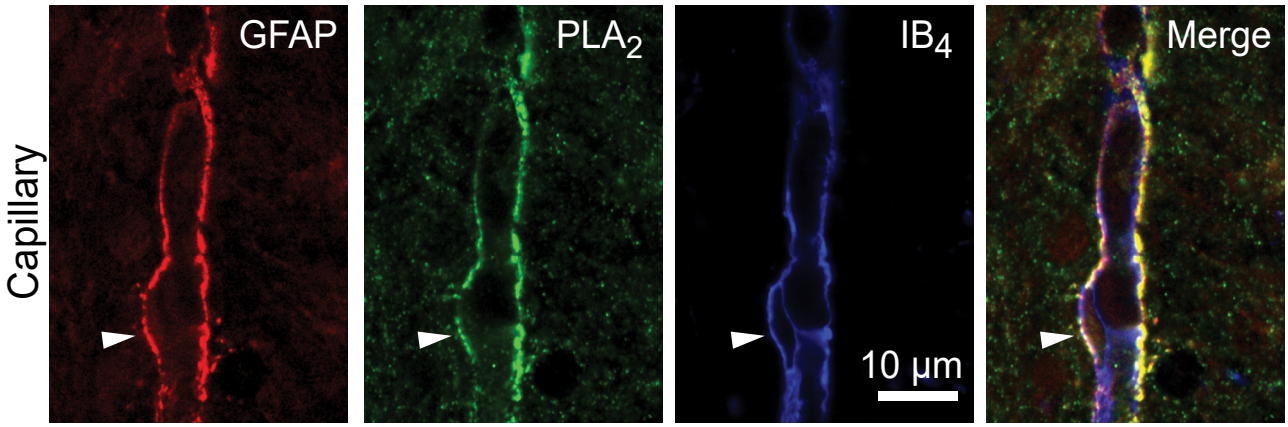

Supplementary Figure 6

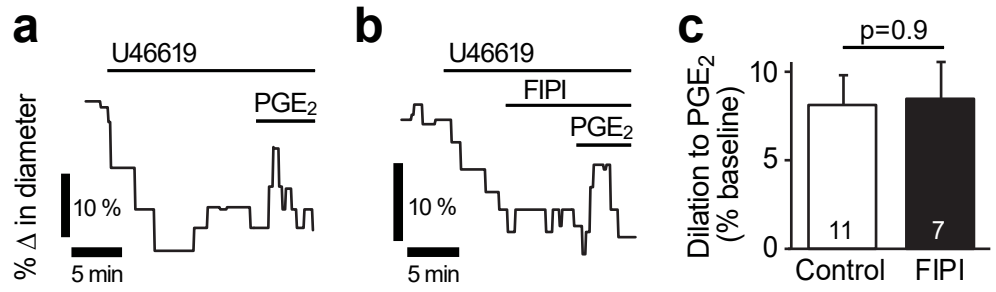

Supplementary Figure 7

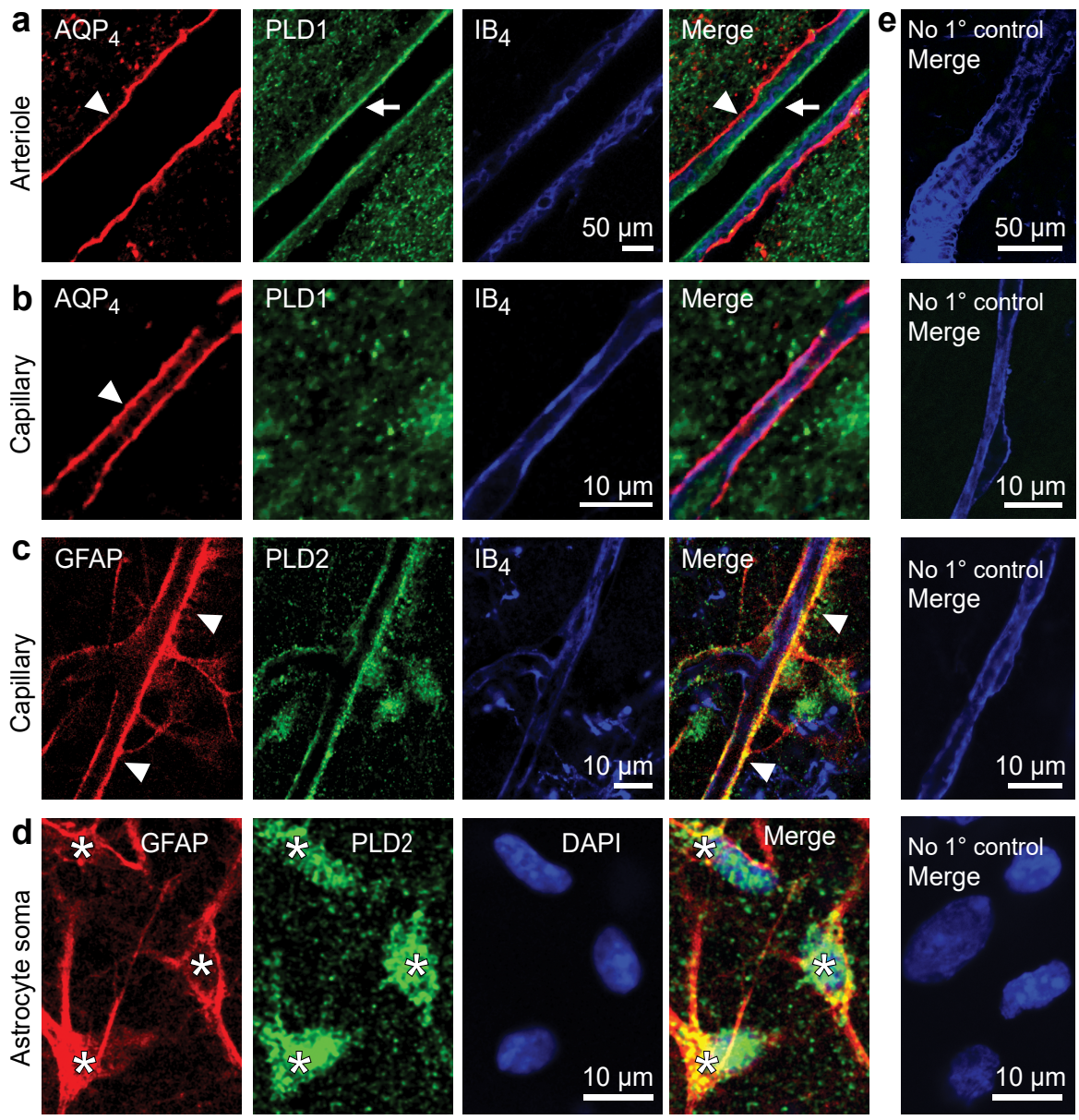

Supplementary Figure 8

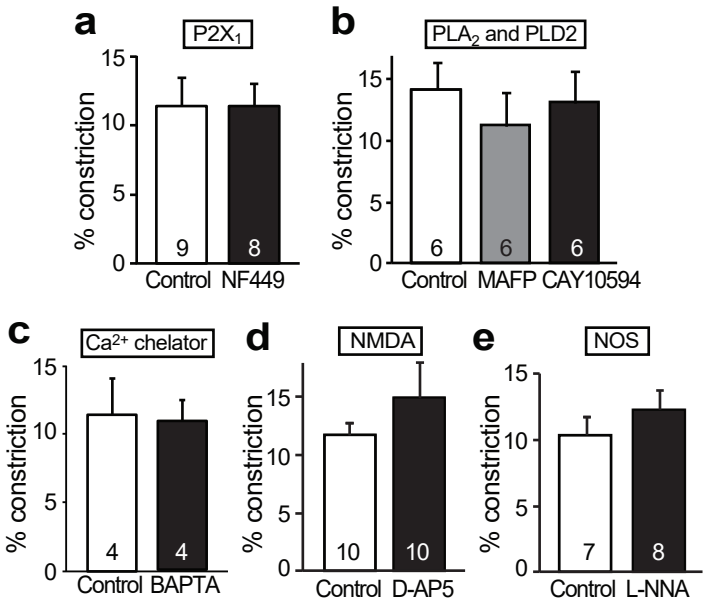

Supplementary Figure 9

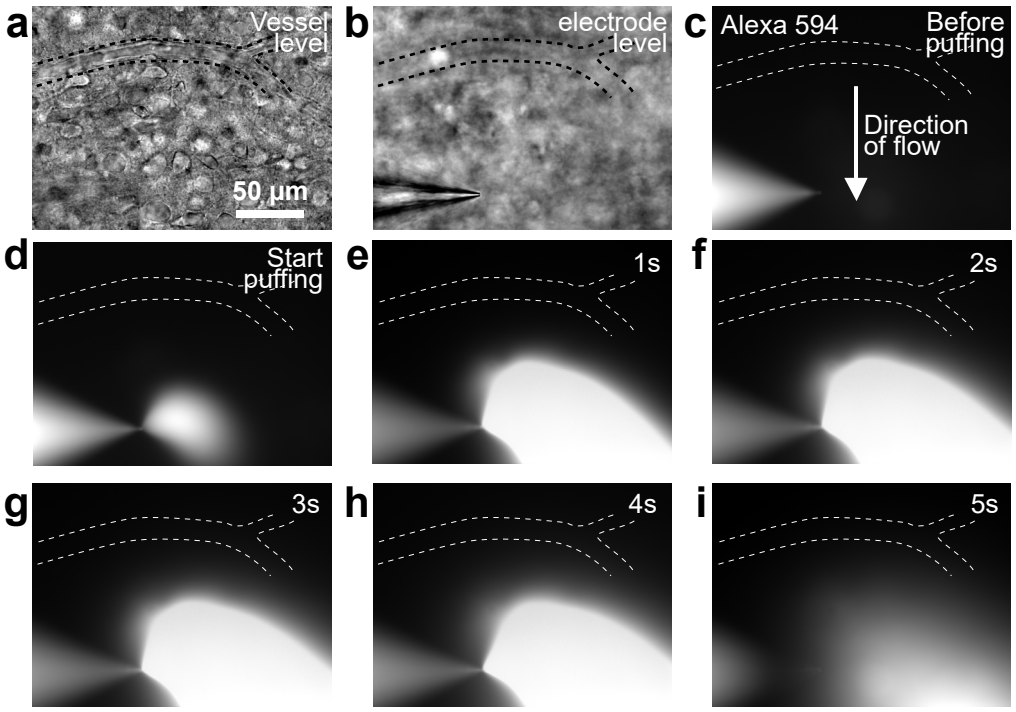

Supplementary Figure 10